NASA Technical Memorandum 101729

A Preliminary Look at Techniques Used to Obtain Airdata From Flight at High Angles of Attack

Timothy R. Moes and Stephen A. Whitmore

December 1990

National Aeronautics and
Space Administration

NASA Technical Memorandum 101729

A Preliminary Look at Techniques Used to Obtain Airdata From Flight at High Angles of Attack

Timothy R. Moes and Stephen A. Whitmore
Ames Research Center, Dryden Flight Research Facility, Edwards, California

1990

National Aeronautics and
Space Administration
Ames Research Center
Dryden Flight Research Facility
Edwards, California 93523-0273

A PRELIMINARY LOOK AT TECHNIQUES USED TO OBTAIN AIRDATA FROM FLIGHT AT HIGH ANGLES OF ATTACK

Timothy R. Moes and Stephen A. Whitmore
NASA Ames Research Center
Dryden Flight Research Facility
Edwards, CA

ABSTRACT

Flight research at high angles of attack has posed new problems for airdata measurements. New sensors and techniques for measuring the standard airdata quantities of static pressure, dynamic pressure, angle of attack, and angle of sideslip were subsequently developed. This report updates the ongoing airdata research supporting NASA's F-18 high alpha research program. Included are the techniques used and the preliminary results. The F-18 aircraft was flown with three research airdata systems: a standard airdata probe on the right wingtip, a self-aligning airdata probe on the left wingtip, and a flush airdata system on the nose cone. The primary research goal was to obtain steady-state calibrations for each airdata system up to an angle of attack of 50°. This goal was accomplished and preliminary accuracies of the three airdata systems were assessed and are presented in this report. An effort to improve the fidelity of the airdata measurements during dynamic maneuvering is also discussed. This involved enhancement of the aerodynamic data with data obtained from linear accelerometers, rate gyros, and attitude gyros. Preliminary results of this technique are presented.

INTRODUCTION

The high alpha research program was established by NASA to investigate issues related to aircraft maneuverability and controllability up to an angle of attack of 70°. Flight tests were conducted at the NASA Ames Research Center's Dryden Flight Research Facility (Ames-Dryden). With this high angle-of-attack flight test program, as with any other flight test program, came the requirement for research quality airdata at all flight conditions. Airdata parameters, such as Mach number, dynamic pressure, angle of attack, and angle of sideslip, are essential for correlating flight data with wind tunnel and computational fluid dynamics data. These parameters are also essential for research in such areas as aircraft performance, handling qualities, stability and control, and flow visualization. The primary goal of this study was to provide information for researchers in these disciplines. An equally important goal was to obtain a better understanding of the physical flow phenomena influencing the airdata measurements. Understanding these phenomena benefits the capability to obtain high-fidelity airdata measurements for use in control system feedback on high-performance aircraft.

Traditionally, the availability of accurate airdata for research flights is taken for granted by many research engineers. The F-18 aircraft production airdata system was not designed to perform well at high angles of attack. Also, standard research airdata systems used by NASA

were not designed for high angle-of-attack flight. Therefore, new sensors and analysis techniques were required to obtain the necessary accuracy in airdata measurements at high angles of attack. This report gives a perspective of the airdata research efforts conducted on the F-18 high alpha research vehicle (HARV) and the preliminary results obtained. Work continues in the effort to understand the accuracies of the airdata systems and the physical phenomena affecting the performance of the airdata systems. The F-18 aircraft was flown with three research airdata systems: a standard NACA airdata probe on the right wingtip, a self-aligning airdata probe on the left wingtip, and a high angle-of-attack flush airdata sensor (HI-FADS) system on the nose cone. Preliminary flight results for these three systems are presented for angles of attack up to 50°. Much work remains to improve our understanding of the performance of these systems.

Also discussed are efforts to improve the frequency response of the airdata estimates by merging airdata measurements with high-frequency inertial information. Such improvement is necessary for high angle of attack and maneuvering flight when the unsteady aerodynamics adversely affect the performance of the airdata systems. This effort is part of ongoing research that will eventually result in real-time airdata feedback into flight control systems. It has significant application in the areas of propulsion and aerodynamic control on modern high-performance aircraft.

NOMENCLATURE

ESP	electronically scanned pressure
HI-FADS	high angle-of-attack flush airdata sensor
HARV	high alpha research vehicle
H_p	pressure altitude
ILS	instrument landing system
INS	inertial navigation system
LKF	linear Kalman filter
M_i	indicated Mach number
M	free-stream Mach number
NACA	National Advisory Committee on Aeronautics
p	free-stream static pressure
p_i	HI-FADS measured pressure at pressure orifice i
POPU	push-over/pull-up
p_t	free-stream total pressure
q_c	free-stream impact pressure $= p_t - p$
rms	root mean square
u, v, w	body-axis components of free-stream velocity
V	free-stream velocity
WLSS	wings-level sideslip
α	true angle of attack

α_{bias}	bias term in computation of $\Delta\alpha_S$
α_i	indicated angle of attack
α_e	HI-FADS effective angle of attack
α_1	α_i corrected for vehicle angular rates
α_2	α_1 corrected for symmetric upwash
β	true angle of sideslip
β_e	HI-FADS effective angle of sideslip
β_F	flank angle of attack
β_{F_i}	indicated flank angle of attack
β_i	indicated angle of sideslip
β_1	β_i corrected for vehicle angular rates
β_2	β_1 corrected for symmetric sidewash
$\Delta\alpha$	HI-FADS upwash calibration parameter
$\Delta\alpha_A$	asymmetric angle-of-attack upwash correction
$\Delta\alpha_S$	symmetric angle-of-attack upwash correction
$\Delta\beta$	HI-FADS sidewash calibration parameter
$\Delta\beta_A$	asymmetric angle-of-sideslip sidewash correction
$\Delta\beta_S$	symmetric angle-of-sideslip sidewash correction
ΔM	Mach number position error correction
$\Delta M_{\text{low-}\alpha}$	component of ΔM for low-α flight
$\Delta M_{\text{high-}\alpha}$	component of ΔM for high-α flight
δM	Mach number residual parameter
$\delta\alpha$	angle-of-attack residual parameter
ε	HI-FADS calibration parameter
ε_M	component of ε due to Mach
ε_α	component of ε due to angle of attack
θ	HI-FADS total flow angle

Subscripts

HI-FADS	nosetip flush airdata sensing system
i	indicated
L	left wingtip swivel probe

R	right wingtip NACA probe
ref	reference

BACKGROUND

A preliminary review of early results on high angle-of-attack airdata research obtained at NASA Ames-Dryden is presented. The review reflects ongoing research in an area that has been largely unexplored. The measurement of airdata in the high angle-of-attack flight regime is difficult for several reasons. These include: (1) the difficulty in obtaining a "truth" set of airdata to calibrate the sensors, (2) problems with the available locations to mount sensors, (3) the nonsteady conditions inherent to high angle-of-attack flight, and (4) the measurement system frequency response.

The need to calibrate airdata sensors arises from the fact that the airflow induced by the aircraft affects the airdata measurements. Calibration implies the comparison of a measurement with a true value. In most cases, however, only estimates of the true airdata are known and the airdata sensors are compared with these estimates. The techniques used to obtain the best estimates of the airdata are discussed in the data analysis section. The accuracy of the estimation techniques used in the analysis vary. Some techniques, such as tower flybys and acceleration-decelerations, have been used for years and are very accurate. In other cases, Kalman filtering techniques (ref. 1) were used to reach the best estimate of the airdata quantities. Mainly, independent sources such as radar data, meteorological data, and inertial instrumentation were used by the Kalman filter to infer the true airdata states. However, in some cases these sources were unavailable or were not suitable for accurate calibrations. The calibrated airdata sensors were used to estimate true airdata for comparison with the airdata sensors. This situation was less than ideal, but was useful for obtaining preliminary information. Improved analysis techniques are being developed to "close-the-loop" on the calibrations with further flight testing. These techniques will not be presented in this paper.

Another difficulty encountered was obtaining good mounting locations for the airdata sensors. Noseboom-mounted airdata systems are typically used to minimize the influence of the aircraft on the airdata measurements. However, a noseboom was deemed unacceptable for this program. At high angles of attack the noseboom has a significant effect on the forebody aerodynamics and thus on the stability and control of the aircraft (ref. 2). As a result, wingtip-mounted sensors and a flush nose cone-mounted sensor were used. The wingtip sensors were placed in regions where a large sidewash and upwash was induced by the aircraft. The local flow at the tip of the aircraft where the HI-FADS sensor was located was also highly affected by upwash. The wings on the F-18 aircraft are very flexible, and they twist and bend as the flight conditions change. Because the motion of the wings was not well known, no adjustments were made to the measurements to account for the deflections. Structural modes of the wings also induced noise on the angle-of-attack and angle-of-sideslip measurements, which correlated well with the first bending and first torsional modes of the wing.

The unsteady conditions associated with high angle-of-attack flight and the low-frequency response of the airdata systems also presented difficulties in obtaining accurate airdata. For all three airdata systems, the performance degraded during rapid maneuvering when the angular

rotation rates were high. The degradation was most significant for the airdata parameters that relied on pressure measurements. This observation was not surprising because the calibrations were done for steady-state effects. The two primary causes for this performance degradation are thought to be (1) unmodeled aerodynamic effects, and (2) acoustical distortion in the pressure-measuring systems. Research has been done on compensation for acoustical distortion (ref. 3). For most cases, the largest part of the error is caused by the unmodeled aerodynamic effects. It was impractical to attempt calibration for the dynamic effects on the airdata systems discussed in this report. Instead, other information sources were used to enhance frequency response of the airdata measurements. This enhancement was important because of the dynamic nature of flying at high angles of attack.

VEHICLE DESCRIPTION

The HARV (fig. 1) is a modified F-18A single-place twin engine fighter–attack aircraft. The aircraft features a variable camber midwing with leading-edge extensions mounted on each side of the fuselage from the wing root to just forward of the windshield. The control surfaces include ailerons, differential stabilators, twin rudders, and multiple flaps. The flap positions were scheduled to a flight control system filtered angle of attack. At angles of attack above approximately 27°, the flaps were set at a specified position and not allowed to move. The wingtip Sidewinder launch racks were removed and replaced with special camera pods that were also used to mount the wingtip research airdata booms. Measurements from these airdata booms were affected by the twisting and bending of the flexible wing.

The fuselage-mounted production F-18 airdata probes were not modified and were used for control system inputs. These measurements were not considered useful for high angle-of-attack flight research because the angle-of-attack probe stopped functioning at 33° and the pressure probes were uncalibrated for high angle-of-attack flight.

The aircraft was also modified to use the instrument landing system indicator needles for trajectory guidance. Trajectory guidance was achieved by uplinking altitude and angle of attack from the ground to the cockpit head-up display to improve the quality of the flight test maneuvers (ref. 4).

INSTRUMENTATION

NACA Airdata Probe

The standard airdata probe flown on most research aircraft at Dryden is known as the NACA probe because it was designed during the National Advisory Committee on Aeronautics era (ref. 5). The probe was installed on the right wingtip boom of the HARV. The NACA probe includes pitot and static pressure orifices as well as angle-of-attack and angle-of-sideslip vane-type flow direction sensors (fig. 2). This probe was designed for flight at low angles of attack.

At low angles of attack, the pressure measurement errors are systematic with Mach number and can be easily determined using traditional calibration methods (ref. 6). For subsonic flight there is negligible total pressure error for the NACA probe up to an angle of attack of 25° (ref. 7). Above an angle of attack of 25°, the probe cannot measure stagnation pressure because the probe

is at a large incidence to the flow. The static pressure orifice arrangement of the NACA probe was developed to make the static pressure error insensitive to an angle of attack up to approximately 15° (ref. 5). Beyond 15°, the NACA probe static pressure error is highly sensitive to both Mach number and angle of attack. There is very little quantitative information available in the literature concerning NACA probe performance at high angles of attack and sideslip. Thus, there were many uncertainties regarding the use of the NACA probe as a means of obtaining calibrated airdata at high angles of attack. These uncertainties are discussed later in the report.

Absolute pressure transducers were used for the total and static pressure measurements. Flexible pneumatic tubing was routed from the static and total pressure orifices to the transducers. The transducers were located in the wing approximately 17 ft from the measurement. Heater blankets were used to maintain operating temperatures near 110 °F. The transducers were determined through ground testing as accurate to ± 0.41 lb/ft^2 with 0.02 lb/ft^2 resolution for the static pressure measurements and to ± 0.82 lb/ft^2 with 0.04 lb/ft^2 resolution for the total pressure measurement.

Swivel Probe

A specially designed, self-aligning airdata probe, the swivel probe, was flight tested on the left wingtip of the HARV (fig. 3). A similar probe was used in NASA's Deep Stall research program (ref. 8). The swivel probe consisted of a combined pitot–static tube with four fins attached to the end of the tube to allow for aerodynamic alignment of the probe with the local flow. Aft of the swivel probe, angle-of-attack and angle-of-sideslip vanes identical to those on the NACA probe were installed. The static orifices of the probe were located 10.3 pitot tube diameters behind the probe tip and 7.4 pitot tube diameters forward of the gimbal hub. There were six static orifices placed at 60° intervals around the tube. As with the NACA probe, the swivel probe static pressure measurements were also affected by the presence of the aircraft. However, it was designed to align itself with the local flow to effectively eliminate total and static pressure losses as a result of local angle-of-attack and angle-of-sideslip effects. The probe swiveled freely for local angles of attack between $-15°$ and 72° and for local angles of sideslip between $\pm 40°$. The probe orientation was not measured in flight. However, in-flight video coverage showed good response of the probe to rapidly changing local flow conditions.

Flow-Direction Vanes

The NACA angle-of-attack and angle-of-sideslip flow-direction vanes (ref. 5) were mounted on both airdata booms (figs. 2 and 3). The vanes were mass balanced to remove gravity effects for alignment with the local velocity vector. The angle-of-attack vane always extended to the left of the boom assembly. This meant that the right wingtip angle-of-attack sensor was inboard of the wingtip, while the left wingtip sensor was outboard of the wingtip.

High Angle-of-Attack Flush Airdata Sensor System

A noseboom was installed for the initial 38 flights of the HARV. However, the noseboom interfered with the forebody flows that significantly affect the stability and control of the aircraft.

Therefore, project requirements necessitated removing the noseboom. The nonintrusive HI-FADS system was thus installed on the tip of the nose cone (fig. 4), leaving the standard F-18 nose cone shape unaltered. The HI-FADS used nine surface pressure measurements located within 1.75 in. of the nosetip. Each pressure orifice was connected to 8 ft of tubing with an inner diameter of 0.06 in.

The HI-FADS surface pressures were measured with a multiport electronically scanned pressure (ESP) module. Included in the module were 32 individually calibrated differential (± 5 lb/in^2) pressure transducers, although only 9 were used for the HI-FADS system. The reference measurement was obtained with the same type of absolute pressure transducer used for the wingtip probes. The measurement was obtained from a 50-in^3 reference tank vented to the interior of the nose cone. The HI-FADS transducers were also wrapped in heater blankets. Under constant temperature conditions the accuracy of the differential transducer was ± 1.4 lb/ft^2 with a 1.4 lb/ft^2 resolution.

Potential resonance and aliasing problems with the HI-FADS pressure measurements were circumvented by careful selection of the pneumatic lines used to transmit pressure impulses from the HI-FADS surface ports to the ESP module. Previous dynamic response data for similar installations and the analysis techniques presented in reference 9 were used to design the pressure measurement system. It was determined that at a representative altitude of 20,000 ft, 8 ft of 0.06-in.-diameter flexible tubing connecting the HI-FADS ports to the ESP module approximated a second-order low-pass filter for the low-frequency range. The natural frequency and damping associated with the installation is calculated using the internal geometry of the pressure line and the transducer (ref. 10). For this configuration at 20,000 ft, the pneumatic lag is approximately 15 msec, which is considered acceptable. Figure 5 shows the calculated frequency response of the pressure sensing configuration for three different altitudes. For an altitude lower than 20,000 ft, the attenuation and lag are less; for a higher altitude they are greater.

Other Instrumentation Hardware

Other research measurements obtained on the HARV included: (1) linear accelerations from a set of body-axis accelerometers; (2) pitch, roll, and yaw attitudes from a gimballed attitude gyro; and (3) three-axis angular velocities from a body-axis rate-gyro package. The accuracy of these sensors was established from the flight data noise band. Root mean square (rms) noise was 0.025 g for the linear accelerometers, 0.2 deg/sec for the three rate gyros, and 0.25° for the three attitudes.

All data were digitally encoded on board using pulse code modulation and telemetered to the ground. The data were then displayed in real time and recorded for postflight analysis. The accelerations, angular rates, and attitudes were recorded at 200 samples/sec, the absolute pressures were recorded at 50 samples/sec, and the HI-FADS pressures were recorded at 25 samples/sec.

FLIGHT TEST PROCEDURES

Various flight techniques were used to establish the airdata calibrations. In all cases multiple maneuvers were flown to determine repeatability of the results. When available, trajectory guidance was used to improve the quality of the maneuver by giving the pilot information on Mach, altitude, and angle of attack.

Tower Flyby Maneuver

The tower flyby technique (ref. 11) was used to calibrate the static pressure measurement at low angles of attack. The tower flyby was accomplished by flying the HARV at constant speed and altitude past a sighting tower. The aircraft flew between 100 and 180 ft above the ground. By measuring the ambient pressure at the tower and sighting the aircraft to within 3 ft of its true altitude, the free-stream static pressure is accurately determined for the aircraft. By making various passes by the tower at different speeds, static pressure error is determined for a wide subsonic Mach range. High angle-of-attack flight calibrations cannot be obtained from this method because the aircraft must be flown at low altitudes to obtain quality measurements.

Acceleration-Deceleration Maneuver

The acceleration-deceleration method (ref. 12) was used to obtain static pressure measurement errors at the higher angles of attack and to verify the calibrations from the tower flybys. This maneuver gives static pressure error over a specified Mach number range. The pilot initiates the constant geometric altitude maneuver from a stabilized low airspeed and accelerates at a constant rate until reaching the maximum airspeed where the deceleration is begun. The deceleration continues until the specified angle of attack is reached. Trajectory guidance is used to enable the pilot to fly the aircraft at a constant geometric altitude until the angle of attack is such that the aircraft begins to lose altitude.

The maneuver is tracked by radar to record the geometric altitude of the aircraft. Local weather balloon data and atmospheric charts are analyzed to obtain the free-stream static pressure at the aircraft location (ref. 13). Static pressure error is then determined by comparing the meteorologically determined static pressure with the indicated static pressure measured by the airdata probe.

Push-Over/Pull-Up Maneuver

Push-over/pull-up (POPU) maneuvers were flown at various Mach and altitude conditions to calibrate the angle-of-attack sensors. The maneuver consisted of the pilot stabilizing the aircraft at the desired Mach and altitude, and thus trim angle of attack. Then a series of three POPUs were performed while reestablishing the desired Mach and altitude between each POPU. Maneuvers were performed at 20,000, 30,000, and 40,000 ft at Mach numbers between 0.3 and 0.9.

Wings-Level Sideslip Maneuvers

The angle-of-sideslip sensors were calibrated during wings-level sideslip (WLSS) maneuvers flown at low to moderate angles of attack. The pilot used both rudder and aileron controls to obtain maximum sideslips at a specified angle of attack and with wings level. The aircraft was oscillated between positive and negative sideslip throughout the maneuver.

Dutch Roll and Wing Rock Maneuvers

The angle-of-sideslip sensors were calibrated at high angle of attack using data from dutch roll and wing rock maneuvers. These maneuvers were required because it was not possible to fly WLSS at high angles of attack. The dutch roll maneuver is flown using yaw and roll control inputs. The pilot flies the aircraft through a series of yawing and rolling motions similar to the standard dutch roll dynamic mode. Wing rock occurs naturally on the F-18 aircraft at angles of attack between 35° and 45° when the flow over the wings and leading-edge extensions produces an alternating asymmetric lift distribution.

DATA ANALYSIS METHODS

Reference Airdata

As discussed previously, a major difficulty with high angle-of-attack flight was finding a "truth" set of airdata parameters to calibrate the research systems. In many of the analysis methods discussed, the reference airdata set used for the calibrations was obtained using a linear Kalman filter (LKF). This minimum variance technique was used to estimate a reference trajectory by blending together various data sources. These data sources included airdata, accelerometers, attitude gyros, rate gyros, meteorologically determined winds, and radar data. Reference values of flow angles and Mach number can be obtained from the reference trajectory. Various applications of this technique are shown in references 14, 15, and 16. Information about the Kalman filter can be obtained from reference 1.

Wingtip Mach Number Corrections

As standard operating procedure, all research aircraft go through a series of flights to calibrate Mach number which is a function of both static and total pressure (ref. 7). These calibrations are needed to take into account the various influences that corrupt the static and total pressure measurements. The measurement of static pressure is influenced by the presence of the boom and the aircraft for both the NACA and swivel probes. This influence is commonly referred to as static pressure position error and must be determined for all flight conditions. The primary source of error in the measurement of total pressure is caused by the inclination of the pitot tube to the local velocity vector. At the high inclination angles, the total pressure probe cannot completely recover the stagnation pressure. The NACA probe measurements, therefore, required adjustments for total pressure errors above a certain local angle of attack. As previously discussed, the swivel probe was developed to alleviate this problem.

Static pressure position error is defined as the difference between the free-stream and local pressures at the static pressure orifices caused by pressure field disturbances that are propagated forward from the aircraft during subsonic flight. Position error is primarily a function of Mach number and lift coefficient (ref. 7). Static pressure position error can be easily transformed into Mach number position error (ref. 13) and is presented in that form in this report. Traditionally, position error is obtained as a function of indicated Mach number. However, with the advent of high angle-of-attack flight research, a high angle-of-attack position error term that is a function of indicated angle of attack only must also be determined.

The tower flyby and acceleration-deceleration maneuvers were used to obtain low and high angle-of-attack position error corrections. Only the decelerations were used for obtaining high angle-of-attack position error because it is difficult for the aircraft to smoothly accelerate from high to low angle of attack. The low angle-of-attack position error correction, $\Delta M_{\text{low-}\alpha}$, is only a function of indicated Mach, and the high angle-of-attack position error correction, $\Delta M_{\text{high-}\alpha}$, is only a function of indicated angle of attack. With these two corrections defined, freestream Mach number is

$$M = M_i + \Delta M_{\text{low-}\alpha} + \Delta M_{\text{high-}\alpha} \tag{1}$$

For indicated angles of attack greater than 25°, a correction was applied to the NACA probe total pressure measurement before computing indicated Mach. This total pressure correction was obtained from reference 7 for the NACA probe. Any error in total pressure not removed by this correction would then deposit into the $\Delta M_{\text{high-}\alpha}$ term.

Wingtip Angle-of-Attack and Angle-of-Sideslip Corrections

The definitions of the flow angles are shown in figure 6. A flowchart showing the steps required to compute angle of attack and angle of sideslip from the indicated flow-direction vane signals is shown in figure 7. The procedure is complex and is described as follows.

Angle of attack is defined as

$$\alpha = \arctan \frac{w}{u}$$

A correction is required to take into account the upwash induced by the aircraft. From flight data, it was empirically observed that the upwash correction can be divided into two components: a symmetric component and an asymmetric component. The symmetric component affects both wingtip sensors in the same direction and is obtained from the POPU maneuvers that were flown at approximately 0° sideslip. The asymmetric component affects the wingtip components of upwash in opposite directions and is obtained from WLSS, dutch roll, and wing rock maneuvers where the angle of attack is held fairly constant. With these two components defined, the equation used to obtain angle of attack from the wingtip sensors is

$$\alpha = \alpha_1 - \Delta\alpha_S + \Delta\alpha_A \tag{2}$$

where α_1 is the indicated angle of attack corrected for vehicle angular rates as described in reference 12 and shown in box 5 of figure 7.

The multiple POPU maneuvers were used to obtain the symmetric upwash correction, $\Delta\alpha_S$. For each POPU, the LKF technique was used to obtain an estimate of true angle of attack. The difference between the LKF estimated true angle of attack and the indicated angle of attack corrected for vehicle angular rates, α_1, was used to establish the symmetric upwash correction, $\Delta\alpha_S$. A plot of $\Delta\alpha_S$ as a function of α_1 is shown in figure 8 for one POPU maneuver. From figure 8, the slope of the linear curve and the intercept α_{bias} are obtained for this Mach and altitude condition. Slope and α_{bias} data from all the POPU maneuvers are tabulated as a function of indicated Mach and pressure altitude. The output of the symmetric upwash tables (box 2 of fig. 7) is then combined with α_1 (box 3 of fig. 7) to obtain the symmetric upwash correction term.

As previously discussed, an asymmetric upwash correction, $\Delta\alpha_A$, is also needed to obtain true angle of attack from equation (2). However, before the asymmetric effects on angle of attack can be accounted for, true angle of sideslip must be determined.

Angle of sideslip is defined as

$$\beta = \arcsin \frac{v}{V}$$

The angle-of-sideslip vane, however, is constrained against rotation about the longitudinal axis. Because of this constraint, at high angles of attack the local flow measured by the angle-of-sideslip vane is considerably different than the local angle of sideslip. Therefore, it is necessary to use the angle β_F, which is known as the flank angle of attack (ref. 17), and defined as

$$\beta_F = \arctan \frac{v}{u}$$

Both β and β_F are shown in figure 6. Indicated angle of sideslip, β_i, is then defined as a function of indicated flank angle of attack, β_{Fi}, and indicated angle of attack, α_i:

$$\beta_i = \arctan(\cos \alpha_i \tan \beta_{F_i})$$

This correction is represented by box 4 of figure 7. After obtaining indicated angle of sideslip, the following equation is used to obtain true angle of sideslip from the wingtip sensors:

$$\beta = \beta_1 + \Delta\beta_S + \Delta\beta_A \tag{3}$$

where β_1 is the indicated angle of sideslip corrected for vehicle rates as described in reference 12 and shown in box 5 of figure 7. The remaining two terms are necessary to correct for induced sidewash. Like the upwash correction, it was empirically determined to separate the sidewash correction into two components: a symmetric component, $\Delta\beta_S$, affecting the sideslip vanes equally but in opposite directions; and an asymmetric component, $\Delta\beta_A$, affecting the sideslip vanes in the same direction. The symmetric component was a function of α_2 only and the asymmetric component was a function of β_2 only, as shown in figure 7. Following this line of reasoning,

$$\beta_2 = \beta_1 + \Delta\beta_S$$

and

$$\beta = \beta_2 + \Delta\beta_A$$

Using the existing instrumentation systems, the LKF technique was found unsatisfactory in obtaining true angle of sideslip to calibrate the angle of sideslip vanes. At high angle-of-attack flight, errors in the meteorological wind data result in excessively large errors in the reference angle of sideslip. This makes it extremely difficult to independently calibrate each of the sideslip sensors using this technique. However, because the wingtip angle-of-sideslip sensors were located at the same fuselage station and at equal distances from the aircraft longitudinal axis, an averaging scheme was used to calibrate the wingtip sensors. This scheme assumes that the true angle of sideslip is the average of the wingtip values.

The symmetric component of sidewash was determined for the entire angle-of-attack range by analyzing deceleration maneuvers from low angle of attack to high angle of attack. Sideslip was held at approximately 0°. The correction term for each wingtip sensor is

$$\Delta\beta_{S_R} = -0.5[\beta_{1_R} - \beta_{1_L}] \qquad \text{(right boom)}$$

$$\Delta\beta_{S_L} = 0.5[\beta_{1_R} - \beta_{1_L}] \qquad \text{(left boom)}$$

The asymmetric sidewash correction was obtained in a very similar manner. Dutch roll, WLSS, and wing rock maneuvers were used in the analysis because the correction is a function of angle of sideslip. In this case, the correction factor was evaluated as the differences between the readings of left and right angle-of-sideslip vanes adjusted for symmetric-induced sidewash.

$$\Delta\beta_{A_R} = -0.5[\beta_{2_R} - \beta_{2_L}] \qquad \text{(right boom)}$$

$$\Delta\beta_{A_L} = 0.5[\beta_{2_R} - \beta_{2_L}] \qquad \text{(left boom)}$$

With true angle of sideslip established, the asymmetric upwash correction of equation (2), $\Delta\alpha_A$, can be evaluated for the wingtip sensors as a function of true angle of sideslip (box 8 of fig. 7). Again, an averaging scheme was used to determine these corrections. In this case, true angle of attack was assumed to be the average of the left and right wingtip values of α_2. This assumption was made although the angle-of-attack vanes were not the same distance from the longitudinal axis of the aircraft. The left boom angle-of-attack vane was 7 in. outboard of the wingtip while the right boom angle-of-attack vane was 7 in. inboard of the wingtip. However, the effect of this small difference was assumed negligible. Therefore, angle of attack is adjusted as follows:

$$\alpha = \alpha_2 + \Delta\alpha_A$$

The correction factors for each boom, $\Delta\alpha_{A_R}$ and $\Delta\alpha_{A_L}$, were obtained from flight data using the equations

$$\Delta\alpha_{A_R} = -0.5[\alpha_{2_R} - \alpha_{2_L}] \qquad \text{(right boom)}$$

$$\Delta\alpha_{A_L} = 0.5[\alpha_{2_R} - \alpha_{2_L}] \qquad \text{(left boom)}$$

As with the asymmetric sidewash corrections, these corrections are evaluated from various maneuvers such as dutch roll, wing rock, and WLSS.

HI-FADS Algorithm

The development and calibration of the HI-FADS airdata algorithm is explained in detail in reference 10. The concept uses multiple nonintrusive pressure measurements to obtain the full set of airdata quantities. Incompressible potential flow around a sphere (ref. 18) was used as a starting point to model the pressures on the HARV nosetip. Flight calibration was then used to adjust the coefficients of the model to take into account compressibility, afterbody effects, and the nonspherical noseshape. The pressure model used is

$$p_i = q_c[\cos^2\theta_i + \varepsilon\sin^2\theta_i] + p$$

where θ_i is the total flow angle at the ith orifice and is a function of the orifice location on the nosecap and effective angle of attack and angle of sideslip. The effective values of angle of attack and angle of sideslip are defined by the total flow angle between the stagnation streamline and the nose cone axis of symmetry.

The calibration parameters $\Delta\alpha$ and $\Delta\beta$ are directly related to aircraft-induced upwash and sidewash at the nose cap and were used to correct the effective flow angles to the free-stream flow angles

$$\alpha_e = \alpha + \Delta\alpha$$

and

$$\beta_e = \beta + \Delta\beta$$

The calibration parameter ε was used to adjust the model for compressible, nonpotential flow at the nonspherical nosetip. During the course of the analysis, it was empirically determined to decompose the calibration factor ε into two components: one that varies as a function of Mach number only (ε_M), and one that varies as a function of effective angle of attack only (ε_α). These components are added together to give

$$\varepsilon = \varepsilon_M + \varepsilon_\alpha$$

Maneuvers used to obtain the calibration parameters $\Delta\alpha$, $\Delta\beta$, ε_M, and ε_α included POPUs, acceleration-decelerations, WLSS, and wing rocks. A reference airdata estimate was obtained for each maneuver using the Kalman filter techniques described previously. The calibration parameters were estimated by substituting the reference airdata into the flow model and obtaining the residuals between the measured and reference pressures. These residuals were used to infer the calibration parameters at each data frame using nonlinear least squares regression.

With the calibration parameters well defined, a recursive algorithm was used to obtain airdata from the HI-FADS system. The algorithm was developed to compute free-stream values of angle of attack, angle of sideslip, static pressure, and impact pressure. All airdata quantities are obtained from these parameters and a total temperature measurement. The algorithm is initialized using wingtip probe airdata. At each data frame, the system is linearized around the airdata estimate of the previous data frame. Using iterative least squares, the change in the free-stream airdata parameters between data frames is obtained. Usually, only two iterations are required to identify the new airdata parameters. For more information on the algorithm, refer to reference 10.

Inertial Enhancement

A general problem occurs with the airdata systems used on the HARV. The calibrations are for steady-state flight and do not account for the unmodeled nonsteady aerodynamic effects during high angle-of-attack flight and the poor frequency response inherent to these airdata systems. Inertial enhancement is used to account for these problems.

Figure 9 shows the pressure altitude measurement from the NACA probe during a POPU with pitch rate exceeding 20 deg/sec. It also shows altitude as measured by ground-based radar during the maneuver.

The performance of the NACA probe is degraded substantially during the high-rate maneuver. Consequently, a technique to improve the fidelity of the airdata measurement has been

developed. This technique uses a Kalman filter (ref. 1) to combine low-frequency-response airdata measurements with high-frequency-response measurements of aircraft attitudes, angular rates, and linear accelerations. The Kalman filter combines this information to give the best estimate of airdata. The estimate was based on knowledge of the state and measurement noise covariances. The state noise is a random disturbance of the system dynamics. It was assumed the state noise consisted entirely of random errors in the accelerometers, rate gyros, and attitude gyros. Therefore, the state noise covariances were set using the sensor accuracies specified in the instrumentation section of this report.

The wind speed and direction are important in establishing the airdata parameters because airdata is wind relative. However, no allowance for the changing wind speed or direction was made in establishing the state noise covariances. This assumes that the wind does not change between airdata measurement updates to the filter. In this procedure, airdata measurement updates were made 10 times/sec with angle of attack, angle of sideslip, airspeed, and pressure altitude from the calibrated NACA probe. Through extensive error analysis, the airdata measurement covariances were defined as a function of angle of attack and angular rates. This allowed the algorithm to lower the weightings on the airdata measurements as the angle of attack or angular rates increased during maneuvers.

RESULTS AND DISCUSSION

Airdata System Calibration

NACA Probe Total Pressure Correction

Both total pressure and static pressure were affected during flight at high angles of attack. Wind tunnel data (ref. 7) were applied to the NACA probe total pressure measurement to see if the total pressure could be adjusted into agreement with the swivel probe measurement. The data in reference 7 (fig. 10(a)) were obtained at Mach 0.26 and are applied as a function of indicated angle of attack only. The data in figure 10(a) beyond 45° were extrapolated from the data in reference 7. Indicated angle of attack was used when correcting the total pressure from the wind tunnel data because the indicated value gave the best indication of the local flow at the pitot port. A typical high angle-of-attack maneuver is used in figure 10(b) to show the effectiveness of the total pressure correction. Note that the wind tunnel correction agrees well with the swivel probe total pressure, although it slightly overcorrects.

NACA Probe Mach Number Correction

The Mach number position-error corrections obtained from tower flybys and acceleration-decelerations are shown for the right wingtip-mounted NACA probe in figure 11. In figure 11(a), the tower flyby and acceleration-deceleration results agree to within 0.003 Mach, except at the low Mach numbers where position error is affected by high angle-of-attack flight. A composite low angle-of-attack position error curve is also shown going through the low angle-of-attack test points. Since by definition the position error is zero at Mach = 0, the low angle-of-attack position error curve is extrapolated to zero at $M_i = 0$.

Data taken during decelerations at different altitudes were corrected for total pressure error and then used to obtain the high angle-of-attack position error correction shown in figure 11(b). The high angle-of-attack position error correction, $\Delta M_{\text{high-}\alpha}$, is obtained by determining the difference between the position error for flight at high angles of attack and the low angle-of-attack position error curve. In figure 11(a), the position error correction as a result of angle of attack, $\Delta M_{\text{high-}\alpha}$ at 25,000 ft, is nearly the same as the correction as a result of angle of attack at 35,000 ft.

An average value of $\Delta M_{\text{high-}\alpha}$ was determined from many maneuvers and is shown in figure 11(b) as a function of indicated angle of attack. Free-stream Mach number for the NACA probe is then computed by using equation (1).

Swivel Probe Mach Number Correction

The swivel probe Mach number position error correction is shown in figure 12 for the swivel probe as a function of indicated Mach. As seen in figure 12(a), the tower flyby and acceleration-deceleration results agree to within 0.003 Mach, except at the low Mach numbers where position error is affected by high angle-of-attack flight. As with the NACA probe, data taken during decelerations at different altitudes were averaged to obtain the high angle-of-attack position error correction. Again, this correction was determined not to be a function of altitude for the conditions flown. Free-stream Mach number for the swivel probe is then computed using equation (1).

Comparing figure 11(b) with figure 12(b), note that the high angle-of-attack position error correction for the right boom is up to three times as large as the swivel probe high angle-of-attack position error correction. This is due to the fact that the swivel probe aligns itself with the local flow so that the static orifices remain normal to the local flow. With the static orifices normal to the local flow, there are no cross-flow effects on the swivel probe pressure measurement as there are with the NACA probe. Therefore, as the aircraft changes angle of attack, the only high angle-of-attack influence on the swivel probe position error is the change in the pressure field at the probe location.

Wingtip Probe Symmetric Angle-of-Attack Correction

For each POPU maneuver flown, a plot similar to figure 8 is obtained using the LKF analysis described previously. By fitting a linear curve to the data shown in figure 8, a slope and α_{bias} is obtained. Compilation of the slope and α_{bias} data for the many indicated Mach and altitude conditions flown are plotted in figures 13 and 14 for the two wingtip booms. Note that there is much scatter in the slope and α_{bias} data. However, trends were identified and curve fits were used to give the best estimate of upwash slope and α_{bias} as a function of indicated Mach. An interesting observation is that the wingtip data are a function of altitude. This is presumed to be the result of the dynamic pressure effects on wingtip deflections and twist that occur during flight. For a given indicated Mach and altitude, the correction for symmetric upwash can then be written

$$\alpha_2 = \alpha_1 - \Delta\alpha_S = \alpha_1 - \frac{\delta\Delta\alpha_S}{\delta\alpha_1}\alpha_1 - \alpha_{bias}$$

where the slope and α_{bias} are functions of indicated Mach and altitude.

Wingtip Probe Symmetric Angle-of-Sideslip Correction

The symmetric sidewash correction was evaluated by plotting $\Delta\beta_S$ as a function of α_2 for both wingtips (fig. 15). Data are shown for decelerations to high angle of attack at altitudes of 25,000 and 35,000 ft. There was no discernable effect of altitude on $\Delta\beta_S$. A second-order polynomial was used to fit the data. The equations for the symmetric sidewash corrections are

$$\Delta\beta_{S_R} = 0.93 + 0.038\alpha_{2_R} + 0.0045\alpha_{2_R}^2 \qquad \text{(right boom)}$$

$$\Delta\beta_{S_L} = -0.94 - 0.038\alpha_{2_L} - 0.0044\alpha_{2_L}^2 \qquad \text{(left boom)}$$

The coefficients for the two wingtip probes are approximately the same magnitude but opposite in sign. This was expected for the symmetric aircraft geometry. Standard deviation from the curve fit was 0.2° for both wingtip probes.

Wingtip Probe Asymmetric Angle-of-Sideslip Correction

The asymmetric corrections were plotted as a function of β_2 and curve fit for each wingtip boom in figure 16. The maneuvers analyzed were WLSS, dutch roll, and wing rock. The equations for the third-order curve fit are as follows. Standard deviation for both wing tips is 0.4°.

$$\Delta\beta_{A_R} = -0.08 - 0.0126\beta_{2_R} - 0.00774\beta_{2_R}^2 + 0.000512\beta_{2_R}^3 \qquad \text{(right boom)}$$

$$\Delta\beta_{A_L} = 0.08 - 0.0212\beta_{2_L} + 0.00430\beta_{2_L}^2 - 0.000249\beta_{2_R}^3 \qquad \text{(left boom)}$$

Wingtip Probe Asymmetric Angle-of-Attack Correction

As discussed previously, true angle of attack was assumed to be the average of right and left wingtip values of α_2. When the results from WLSS, dutch roll, and wing rock maneuvers were plotted as a function of angle of sideslip, it was determined that a simple linear regression could be used to fit the data. Again, a considerable amount of scatter existed, but the linear trend was identifiable. The wingtip asymmetric angle-of-attack calibration data, plotted as a function of true angle of sideslip, are presented in figure 17. The linear fits are as follows:

$$\Delta\alpha_{A_R} = 0.09(\beta_R)$$

$$\Delta\alpha_{A_L} = -0.10(\beta_L)$$

HI-FADS Calibration

As discussed previously, calibration maneuvers for the HI-FADS system included POPUs, acceleration-decelerations, WLSS, and dutch rolls. Calibration parameters $\Delta\alpha$, $\Delta\beta$, ε_M, and ε_α were obtained from a nonlinear regression on the residuals between measured pressures and reference pressures. Systematic trends were identified by plotting the estimated calibration parameters against various flight variables.

Calibration curves for the upwash parameter $\Delta\alpha$ are shown (fig. 18(a)) as a function of effective angle of attack. This parameter showed no clearly discernable trend with either Mach number or angle of sideslip. Similarly, calibration curves for the sidewash parameter $\Delta\beta$ are shown (fig. 18(b)) as a function of effective angle of sideslip. This parameter showed no discernable trend with either Mach number or angle of attack. The calibration parameters ε_M and ε_α are shown plotted in figures 18(c) and 18(d).

Airdata System Performance

The performance of the airdata systems was analyzed using the reference airdata generated by the Kalman filter techniques explained previously. An evaluation flight maneuver is used to demonstrate the performance of the airdata systems. The maneuver time history of angle of attack, angle of sideslip, pressure altitude, and free-stream Mach is shown in figure 19. This maneuver consisted of dutch roll and wing rock at low, medium, and high angles of attack.

Residual analysis was done to show the difference between the airdata system and the reference airdata values of angle of attack and Mach. The residual parameters are defined as

$$\delta\alpha_{\text{HI-FADS}} = \alpha_{\text{HI-FADS}} - \alpha_{ref}$$

$$\delta\alpha_R = \alpha_R - \alpha_{ref}$$

$$\delta\alpha_L = \alpha_L - \alpha_{ref}$$

$$\delta M_{\text{HI-FADS}} = M_{\text{HI-FADS}} - M_{ref}$$

$$\delta M_R = M_R - M_{ref}$$

$$\delta M_L = M_L - M_{ref}$$

and are shown (fig. 20) for the evaluation maneuver as a function of angle of attack.

Statistical analysis is used to quantify the errors. The residual mean and root mean square (rms) errors are shown for the three angle-of-attack regions of the demonstration maneuver in the following table.

	$\alpha_{\text{HI-FADS}}$, deg		α_R, deg		α_L, deg	
	Mean	rms	Mean	rms	Mean	rms
$\alpha < 20°$	0.01	0.13	0.08	0.17	−0.08	0.16
$20° < \alpha < 35°$	0.38	0.46	0.06	0.35	−0.18	0.38
$\alpha > 35°$	0.29	0.67	−0.1	0.38	0	0.34
	$M_{\text{HI-FADS}}$		M_R		M_L	
	Mean	rms	Mean	rms	Mean	rms
$\alpha < 20°$	−0.0016	0.0034	−0.0025	0.0030	−0.0022	0.0028
$20° < \alpha < 35°$	−0.0031	0.0039	0.001	0.0020	−0.0026	0.0033
$\alpha > 35°$	−0.0017	0.0032	0.0033	0.0057	−0.0005	0.0028

All three systems measured angle of attack to within 1° and Mach number to within 0.01. In most instances, the rms errors increased with angle of attack. As stated earlier, the performance of these systems is based on steady-state calibrations. Therefore, the performance degrades during higher rate maneuvering.

Inertial Enhancement

The degraded performance of the airdata systems during higher rate maneuvering was cause for investigating a technique to enhance the airdata system performance during maneuvering. The technique chosen, and presently being developed at Ames-Dryden, was a Kalman filtering scheme that used aircraft attitudes, angular rates, and linear accelerations to enhance the airdata measurements. Results of this technique are shown (fig. 21) for the same maneuver presented in figure 9. The enhanced airdata pressure altitude from the NACA boom agrees well with the radar altitude measurement. This technique is equally applicable to the HI-FADS and swivel probe airdata measurements. It shows promise of offering improved airdata frequency response characteristics using conventional airdata systems.

CONCLUDING REMARKS

A significant goal of NASA's F-18 high alpha research program was to obtain accurate airdata for flight at high angles of attack. Data were presented on NASA's F-18 high alpha research vehicle (HARV) for flight up to 50° angle of attack and ±15° angle of sideslip. Although these results were obtained for the HARV, the techniques and analysis methods should still be of interest to designers, developers, and researchers of any high angle-of-attack capable aircraft.

Three airdata systems were flown on the aircraft: a standard NACA airdata probe on the right wingtip, a swivel probe on the left wingtip, and a high angle-of-attack flush airdata sensing (HI-FADS) system on the nose. Each system was capable of obtaining a calibrated Mach number to within ±0.01 and flow angles to within ±1° for angles of attack up to 50°. The swivel probe performed better than the NACA probe in measuring Mach and altitude at high angles of attack because of its self-aligning capabilities. The HI-FADS system performed as well as the swivel probe throughout the angle-of-attack range. None of the airdata systems performed well during high-rate maneuvering. An inertial enhancement technique is being developed to improve the airdata sensor performance during dynamic maneuvering. This technique uses information from

onboard accelerometers, rate gyros, and attitude gyros and shows promise for providing real-time, high-fidelity airdata for all flight conditions using conventional airdata systems.

REFERENCES

1. Lewis, Frank L.: Optimal Estimation With an Introduction to Stochastic Control Theory. John Wiley & Sons, 1986.

2. Fisher, David F.; Richwine, David M.; and Banks, Daniel W.: Surface Flow Visualization of Separated Flows on the Forebody of an F-18 Aircraft and Wind-Tunnel Model. NASA TM-100436, 1988.

3. Whitmore, Stephen A.; and Leondes, Cornelius T.: Compensating for Pneumatic Distortion in Pressure Sensing Devices. NASA TM-101716, 1990.

4. Meyer, R. R.; and Schneider, E. T.: Real-Time Pilot Guidance System for Improved Flight Test Maneuvers. AIAA-83-2747, Nov. 1983.

5. Richardson, Norman R.; and Pearson, Albin O.: Wind-Tunnel Calibrations of a Combined Pitot-Static Tube, Vane-Type Flow-Direction Transmitter, and Stagnation-Temperature Element at Mach Numbers From 0.60 to 2.87. NASA TN-D-122, 1959.

6. Larson, Terry J.; Stillwell, Wendell H.; and Armistead, Katharine H.: Static-Pressure Error Calibrations for Nose-Boom Airspeed Installations of 17 Airplanes. NACA RM H57A02, 1957.

7. Gracey, William: Measurement of Aircraft Speed and Altitude. NASA RP-1046, 1980.

8. Sim, Alex G.: Flight Characteristics of a Modified Schweizer SGS 1-36 Sailplane at Low and Very High Angles of Attack. NASA TP-3022, 1990.

9. Whitmore, Stephen A.: Formulation of a General Technique for Predicting Pneumatic Attenuation Errors in Airborne Pressure Sensing Devices. NASA TM-100430, 1988.

10. Whitmore, Stephen A.; Moes, Timothy R.; and Larson, Terry J.: Preliminary Results From a Subsonic High Angle-of-Attack Flush Airdata Sensing (HI-FADS) System: Design, Calibration, and Flight Test Evaluation. NASA TM-101713, 1990.

11. DeAnda, Albert G.: AFFTC Standard Airspeed Calibration Procedures. AFFTC-TIH-81-5, June 1981.

12. Haering, Edward A., Jr.: Airdata Calibration of a High Performance Aircraft for Measuring Atmospheric Wind Profiles. NASA TM-101714, 1990.

13. Johnson, J. Blair; Larson, Terry J.; and Ficke, Jules M.: Digital Program for Calculating Static Pressure Position Error. NASA TM-86726, 1987.

14. Whitmore, Stephen A.: Reconstruction of the Shuttle Reentry Air Data Parameters Using a Linearized Kalman Filter. AIAA 83-2097, Aug. 1983.

15. Whitmore, Stephen A.; Larson, Terry J.; and Ehernberger, L. J.: Air Data Position-Error Calibration Using State Reconstruction Techniques. NASA TM-86029, 1984.

16. Whitmore, Stephen A.: Formulation and Implementation of a Nonstationary Adaptive Estimation Algorithm With Applications to Airdata Reconstruction. NASA TM-86727, 1985.

17. Maine, Richard E.; and Iliff, Kenneth W.: Application of Parameter Estimation to Aircraft Stability and Control. NASA RP-1168, 1986.

18. Kuethe, Arnold M.; and Chow, Cheun-Yen: Foundation of Aerodynamics: Bases of Aerodynamic Design, Fourth ed. John Wiley & Sons, 1986.

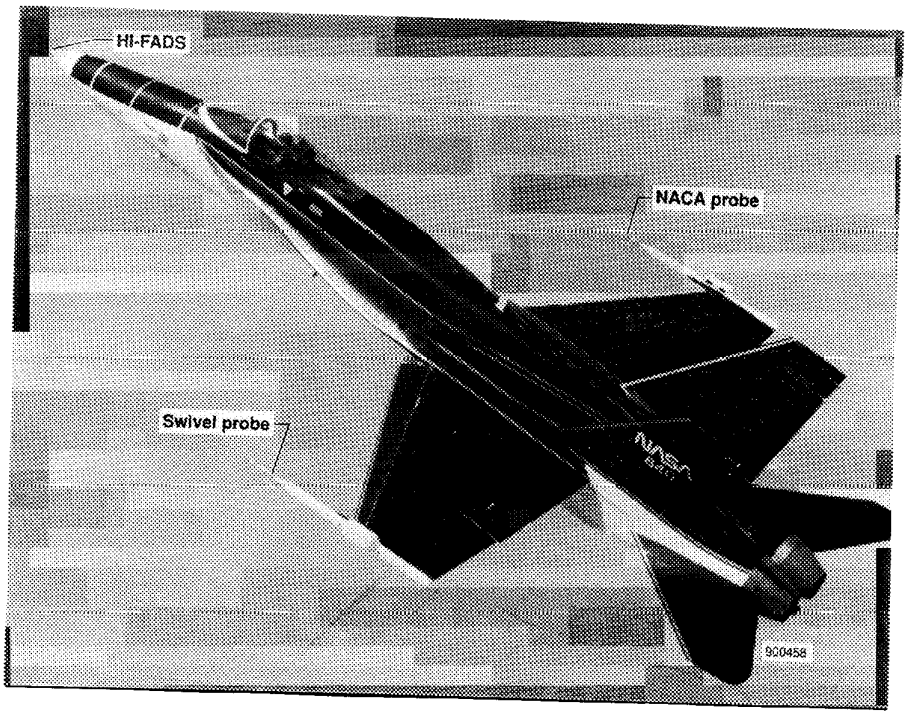

Figure 1. The F-18 high alpha research vehicle.

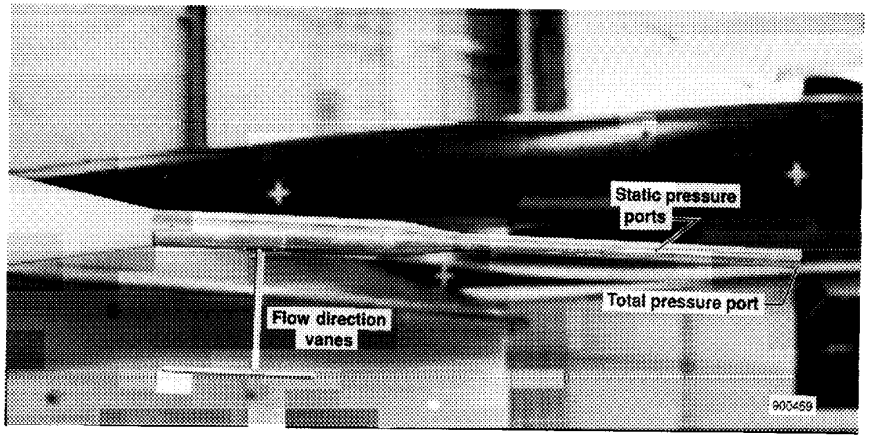

Figure 2. NACA airdata probe.

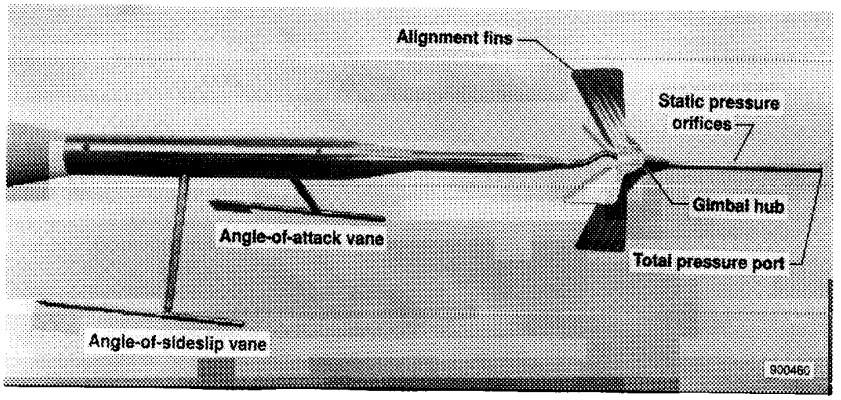

Figure 3. Self-aligning airdata probe (swivel probe).

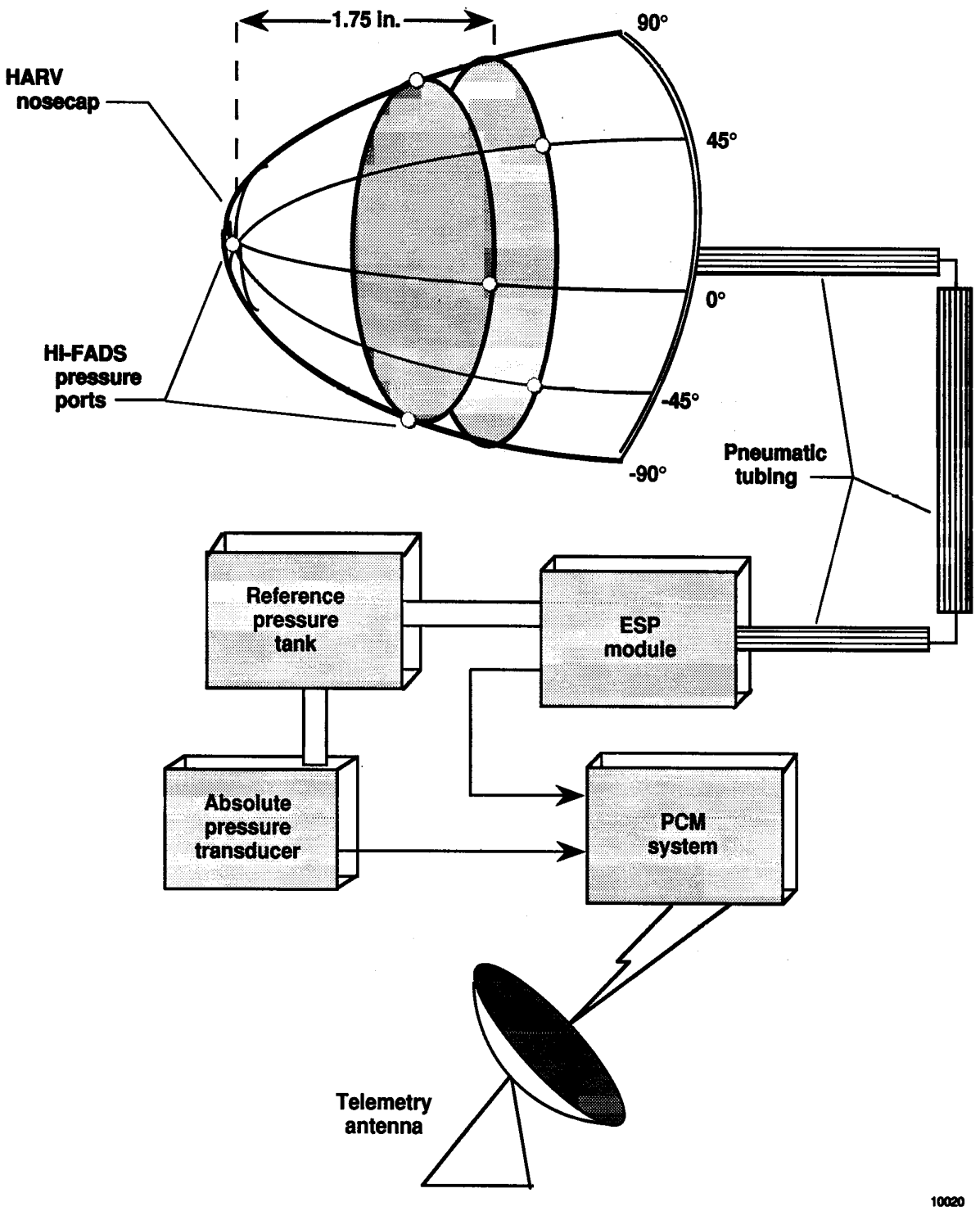

Figure 4. The HI-FADS system.

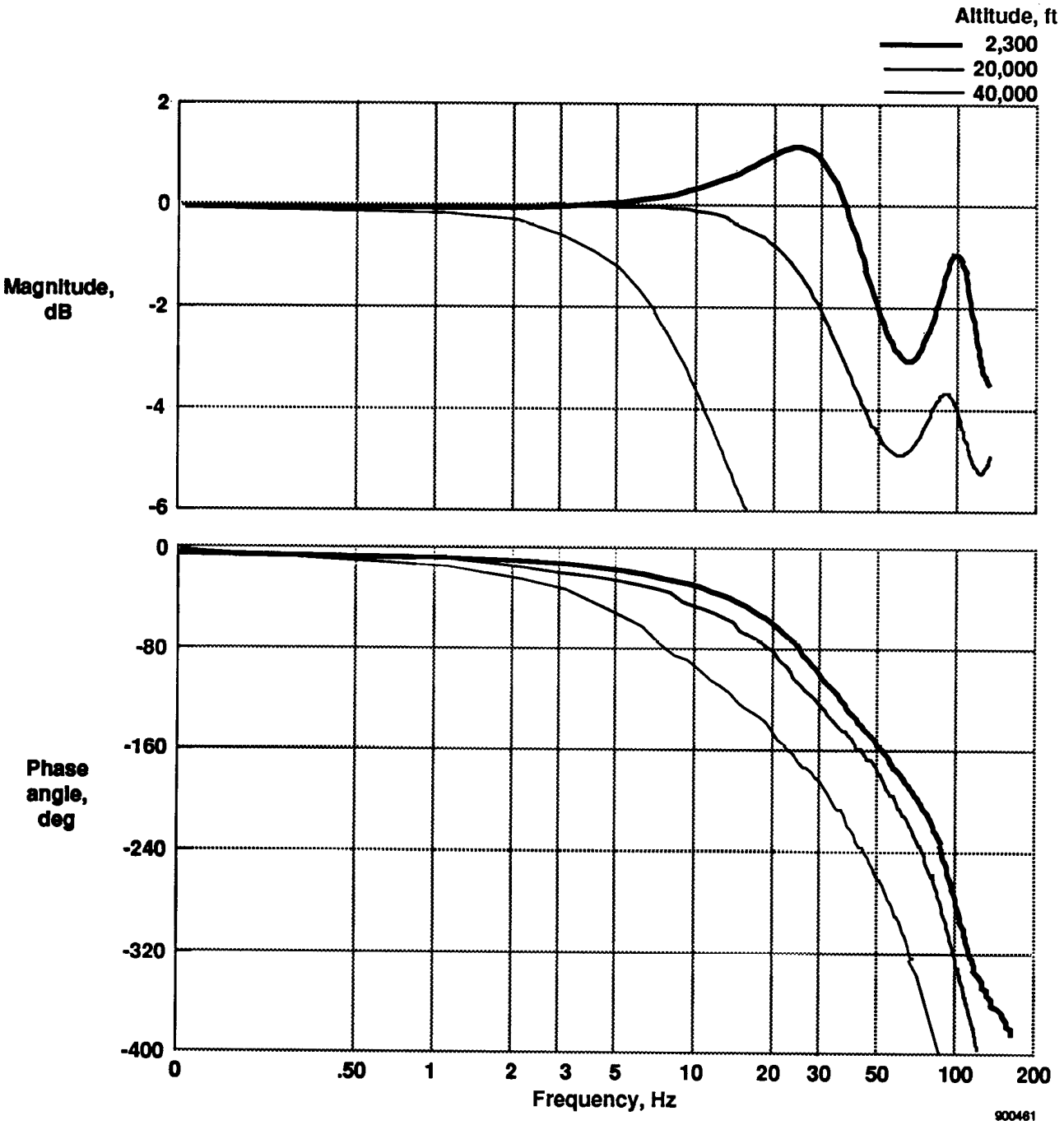

Figure 5. Comparisons of HI-FADS pressure sensor frequency response at 2,300, 20,000, and 40,000 ft altitudes.

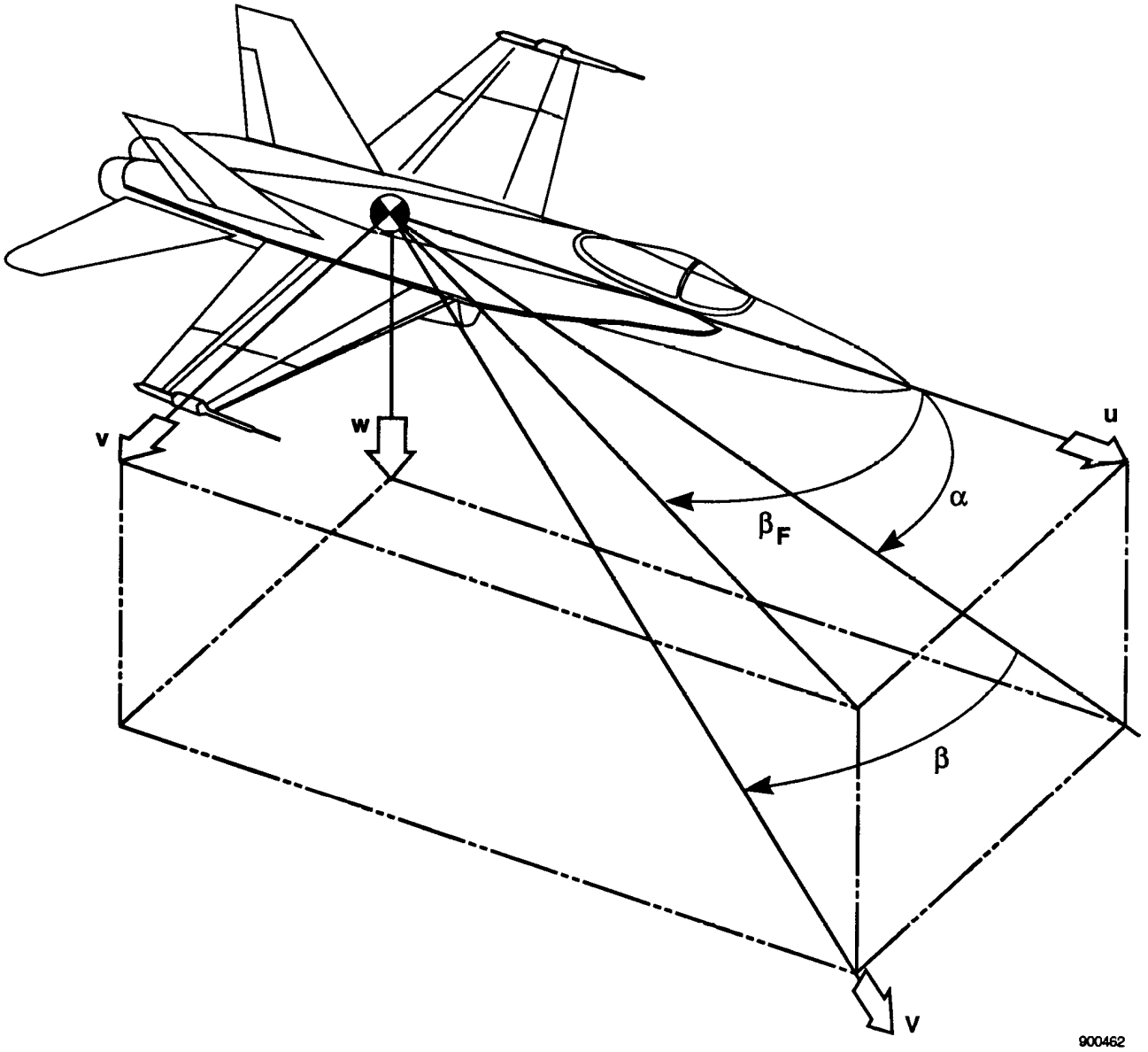

Figure 6. Flow angle definitions.

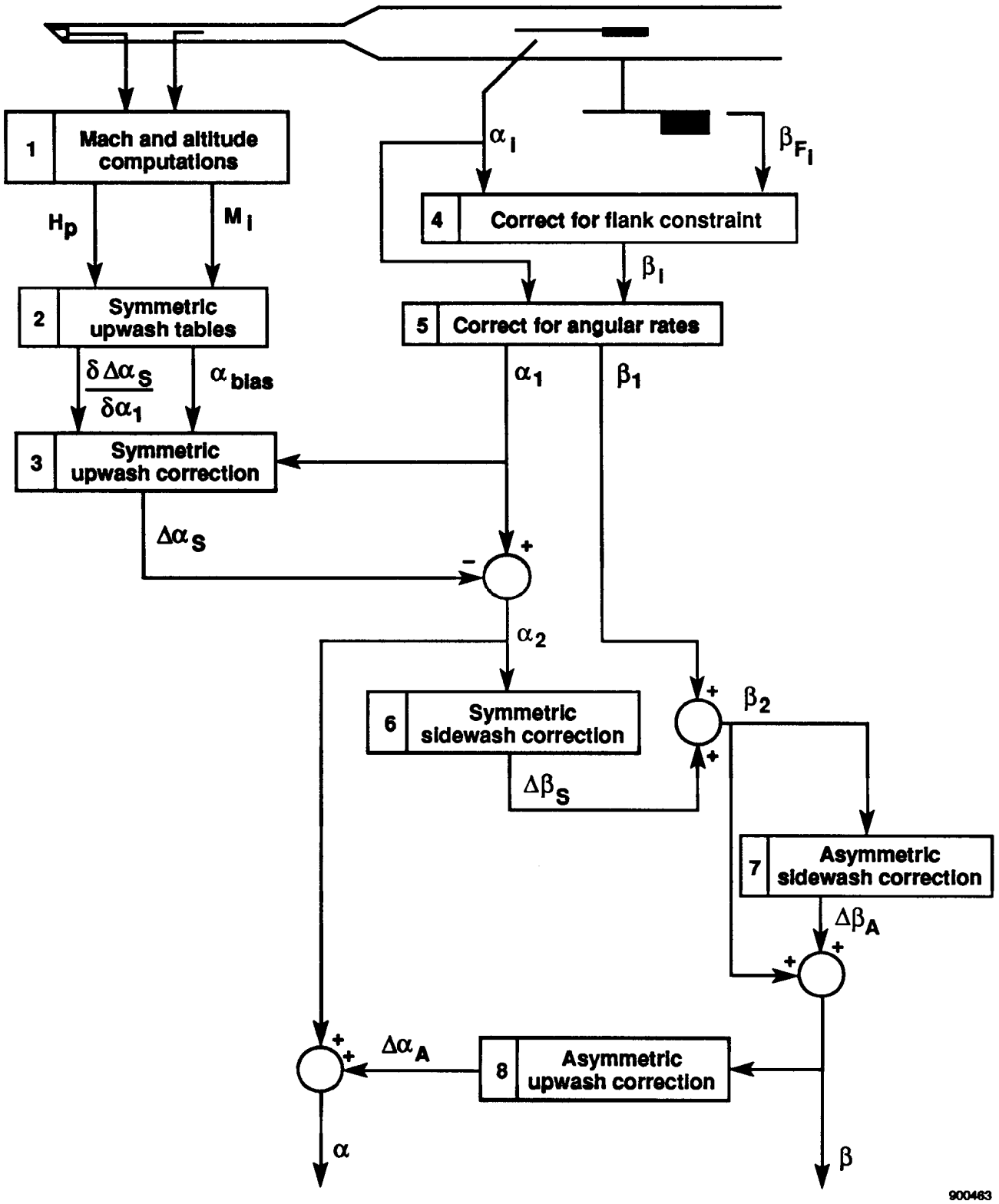

Figure 7. Angle-of-attack and angle-of-sideslip correction scheme flowchart.

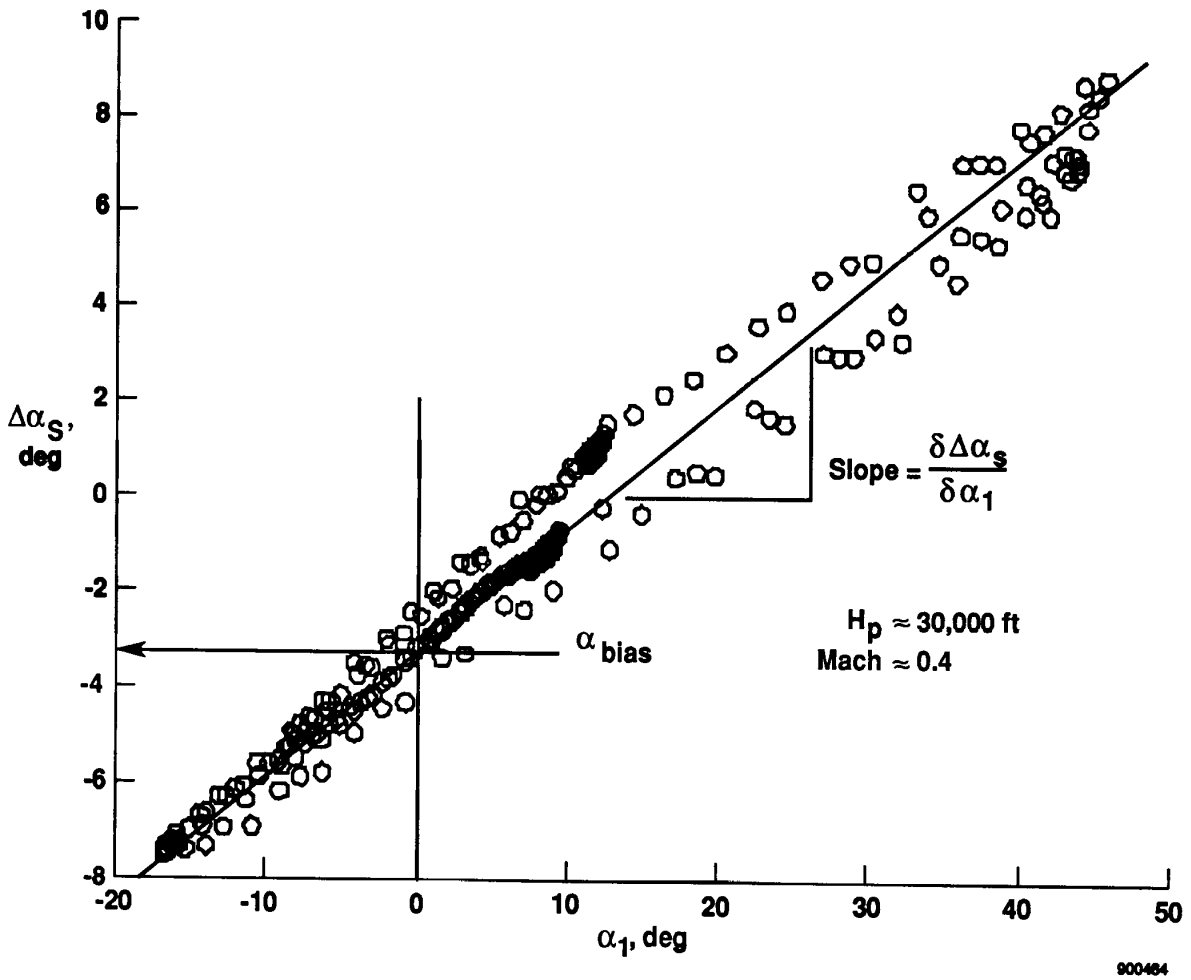

Figure 8. Symmetric upwash effect on angle of attack during a POPU maneuver.

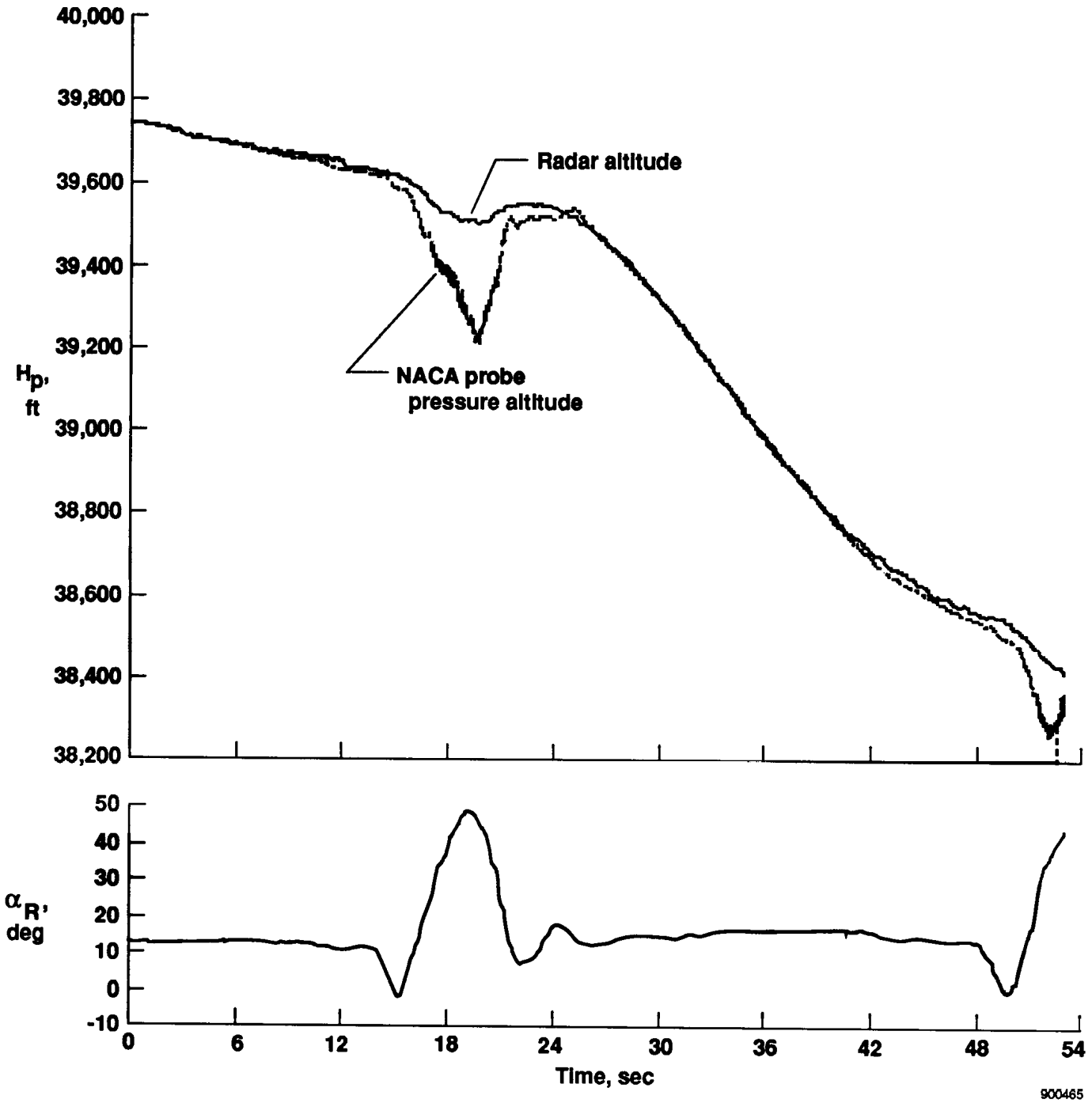

Figure 9. Time history of NACA H_p during a high-rate maneuver.

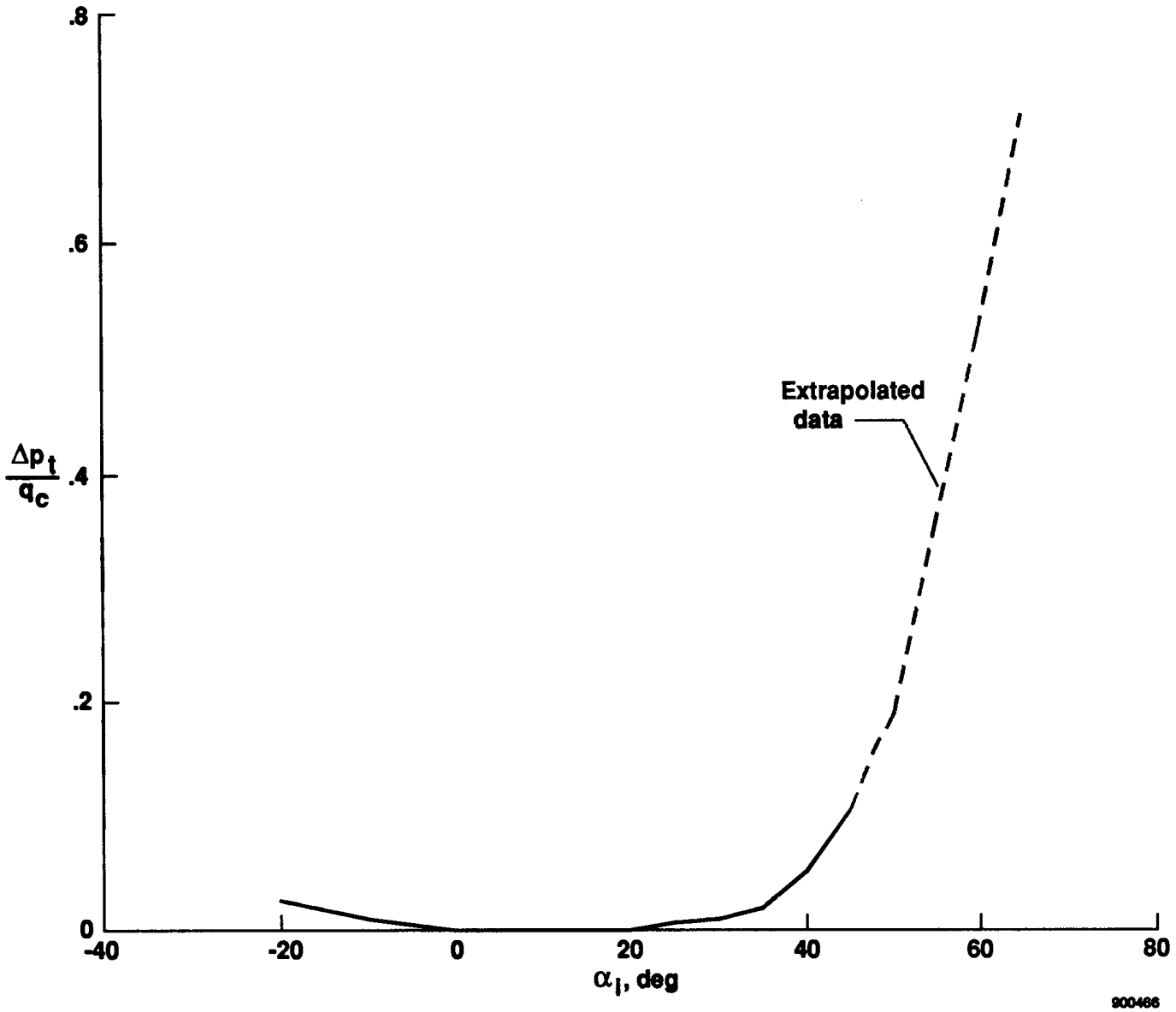

(a) Wind tunnel correction.

Figure 10. NACA probe total pressure correction.

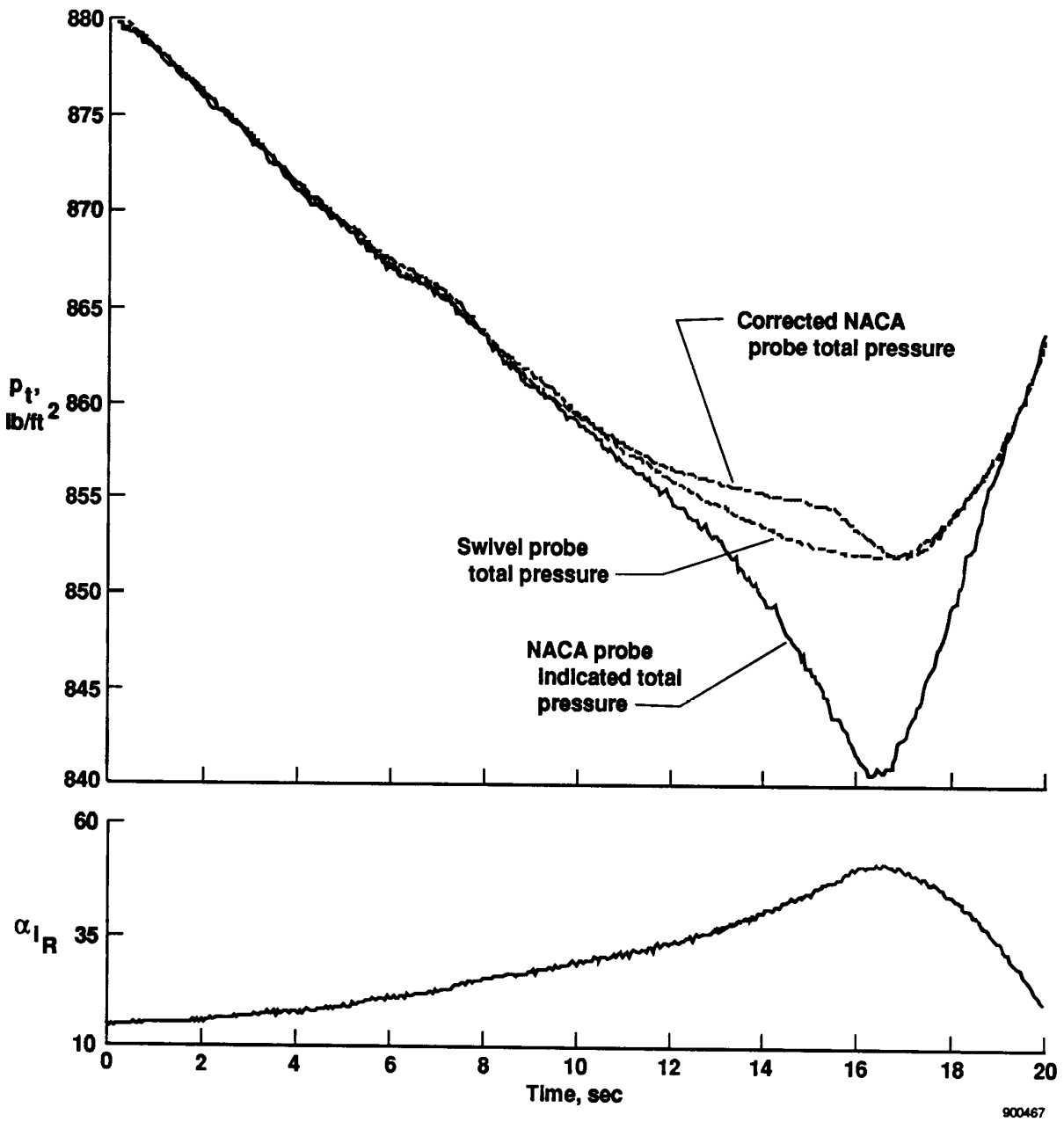

(b) Application to flight data.

Figure 10. Concluded.

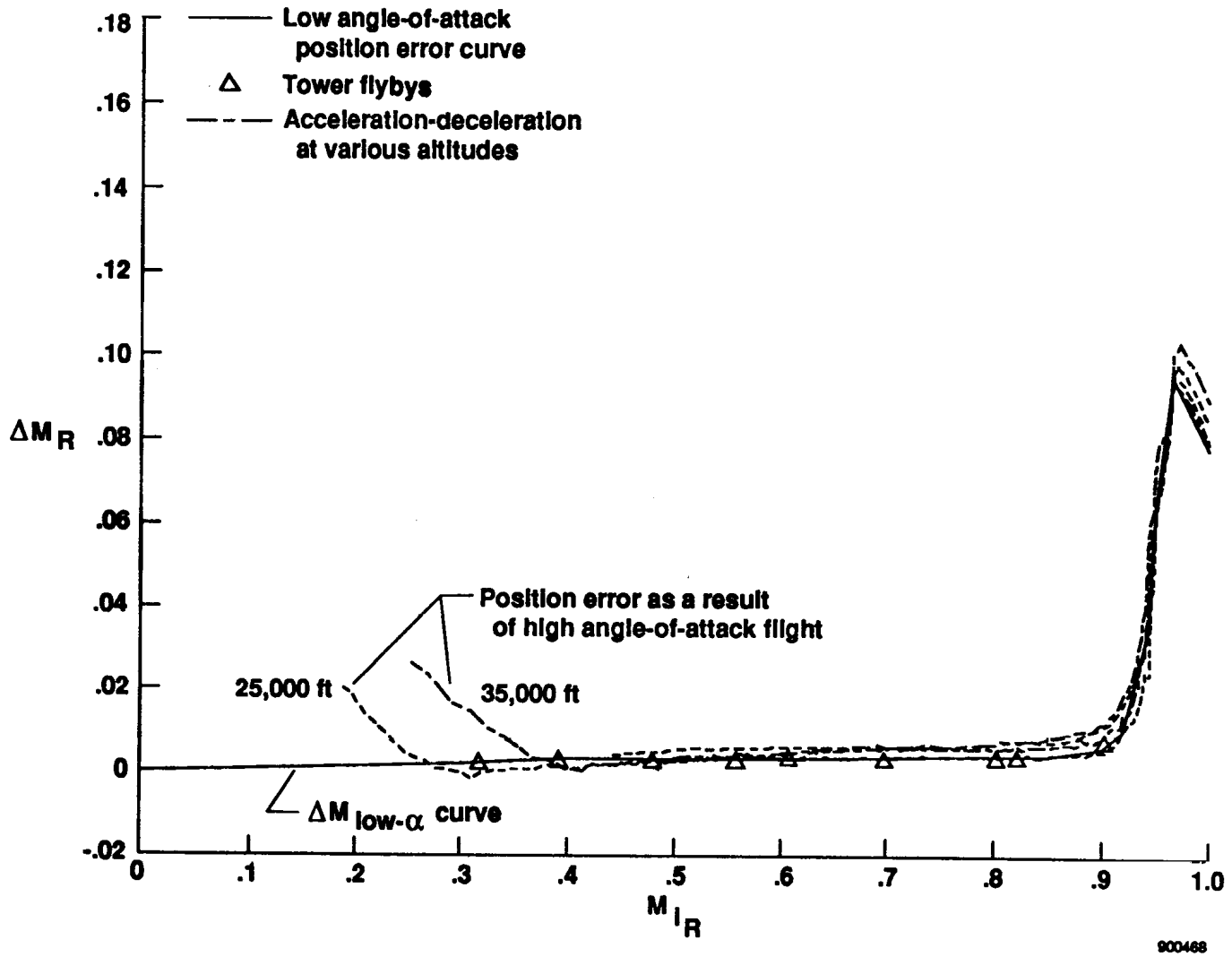

(a) NACA probe position error curve.

Figure 11. Mach number position error for the NACA probe.

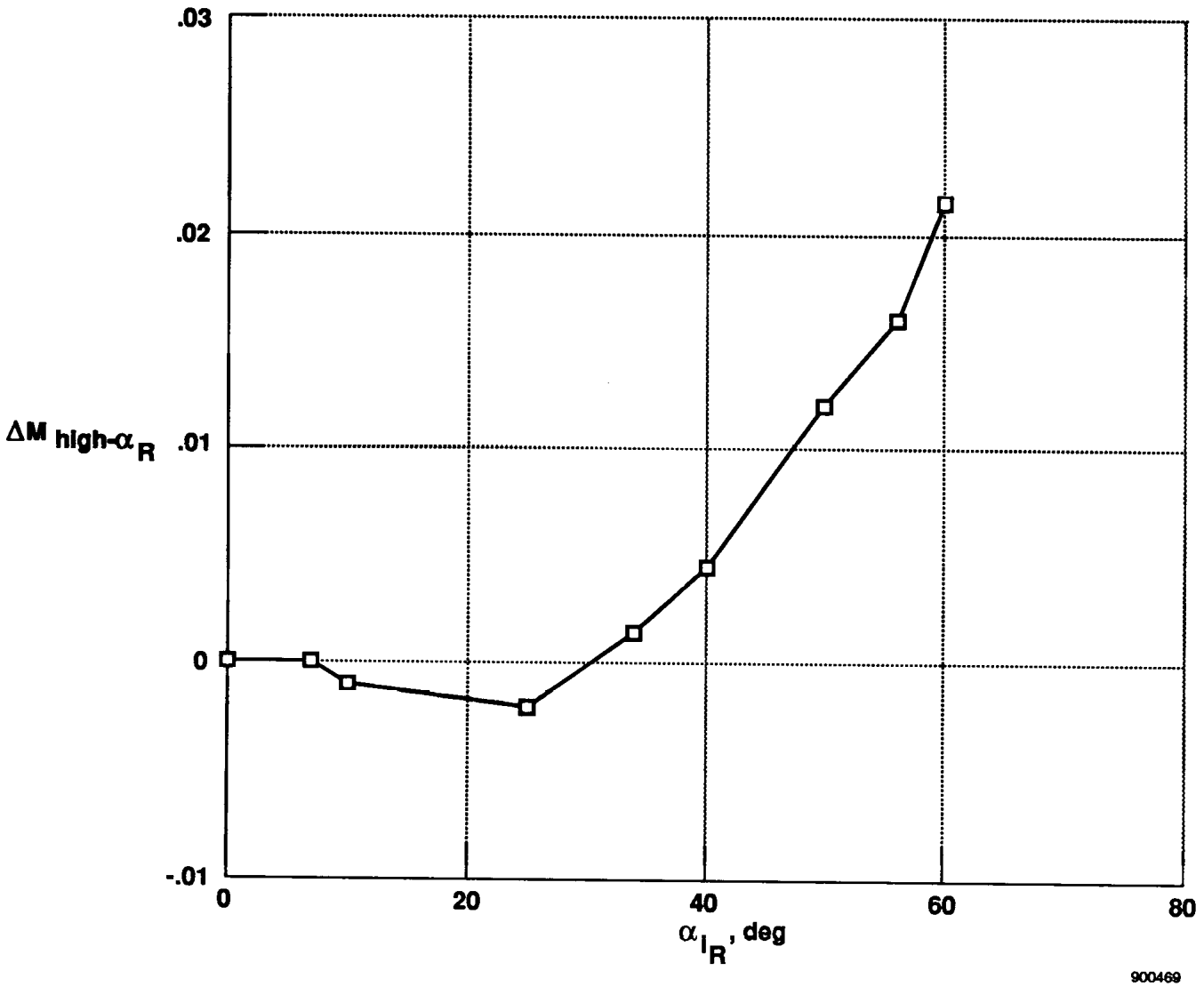

(b) NACA probe high angle-of-attack position error.

Figure 11. Concluded.

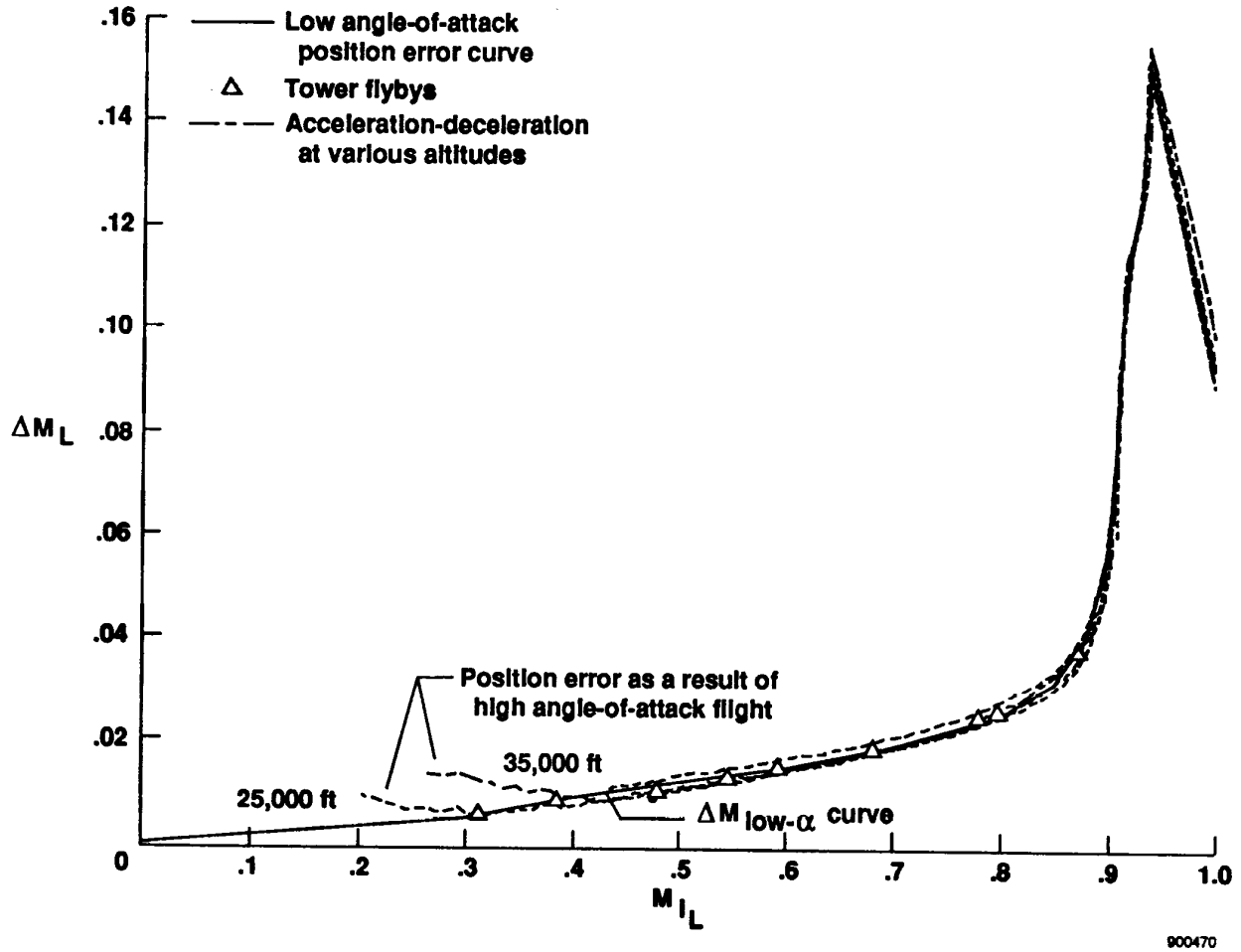

(a) Swivel probe position error curve.

Figure 12. Mach number position error for the swivel probe.

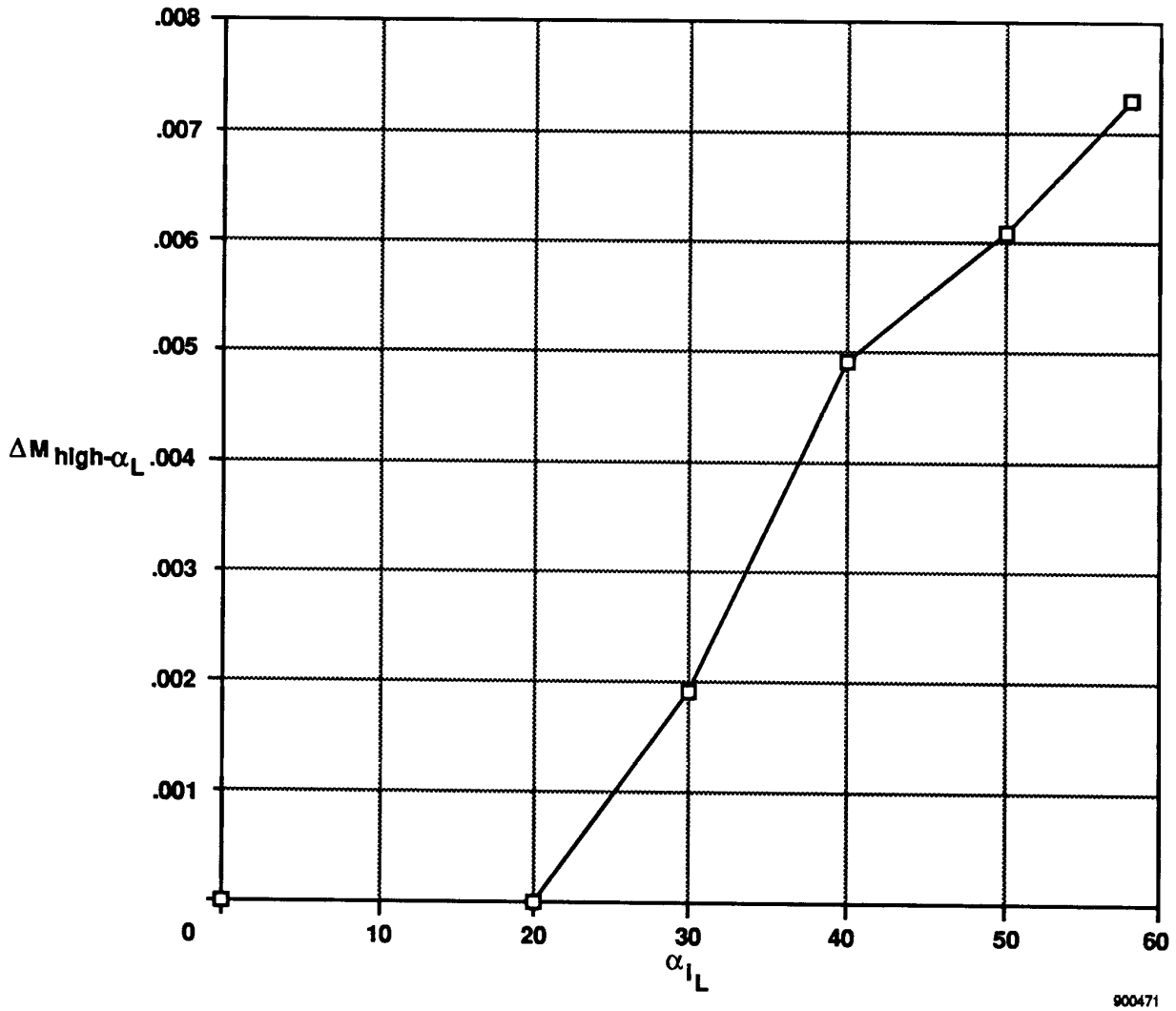

(b) Swivel probe high angle-of-attack position error.

Figure 12. Concluded.

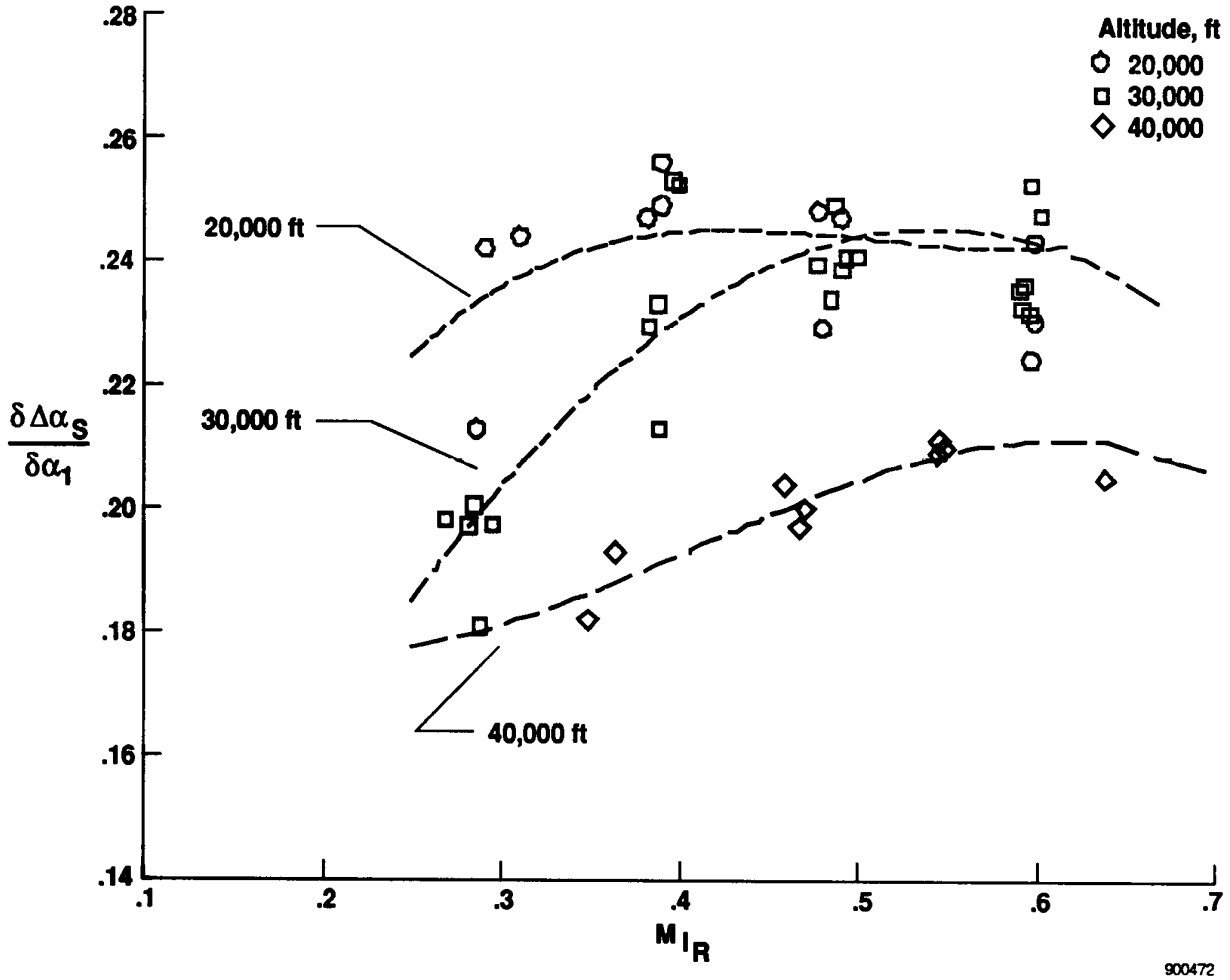

(a) $\frac{\delta\Delta\alpha_s}{\delta\alpha_1}$.

Figure 13. Symmetric upwash corrections for the right wingtip angle-of-attack sensor.

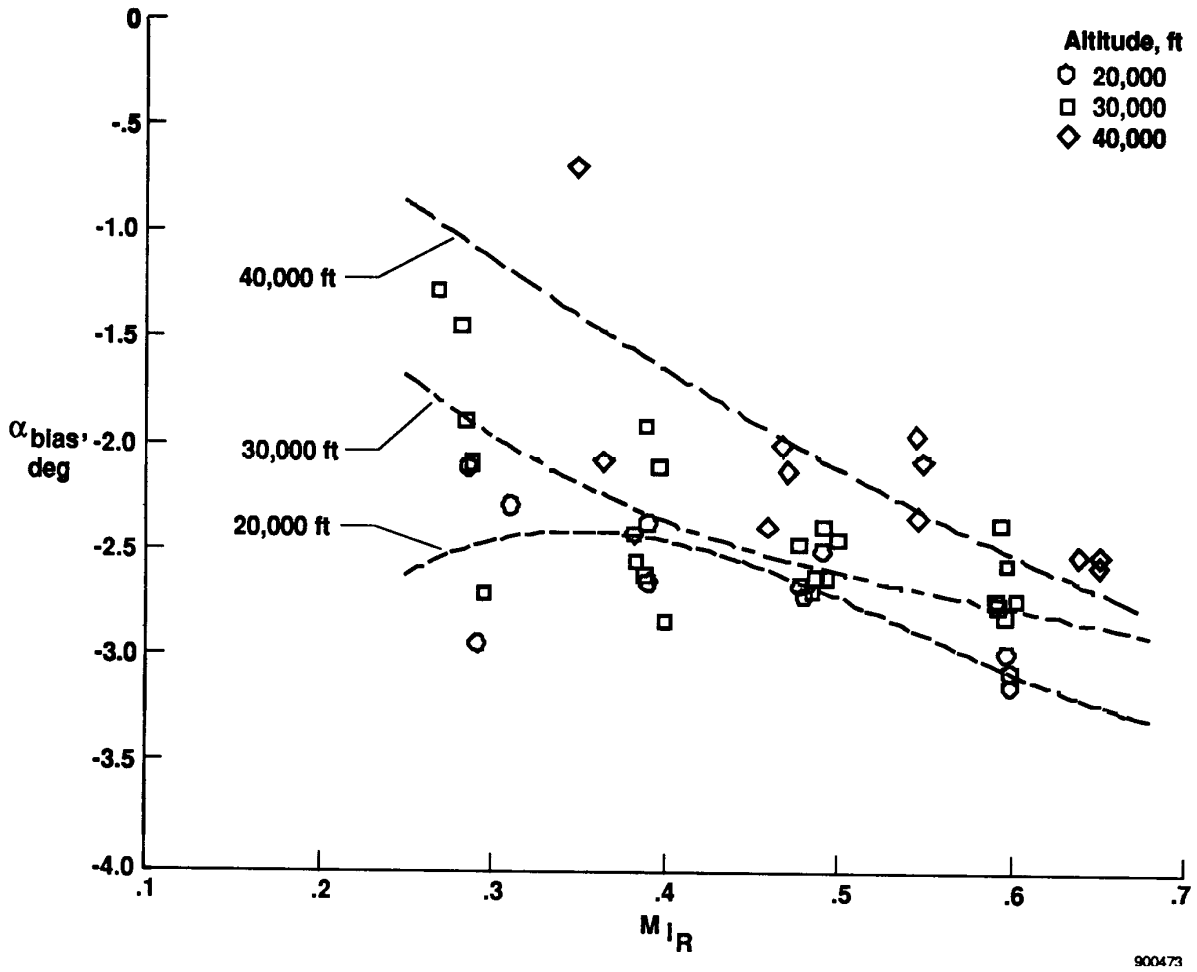

(b) α_{bias}.

Figure 13. Concluded.

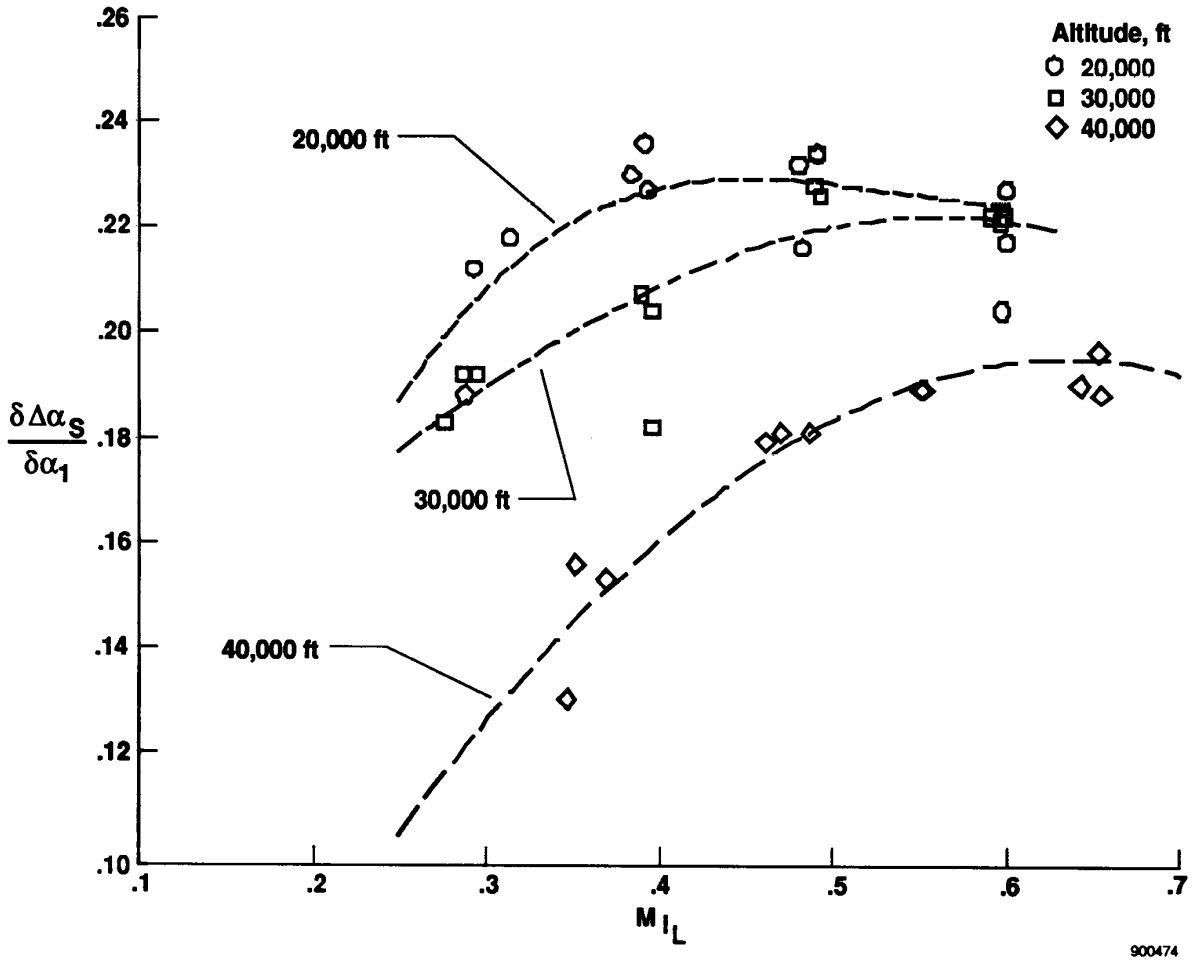

(a) $\frac{\delta\Delta\alpha_s}{\delta\alpha_1}$.

Figure 14. Symmetric upwash corrections for the left wingtip angle-of-attack sensor.

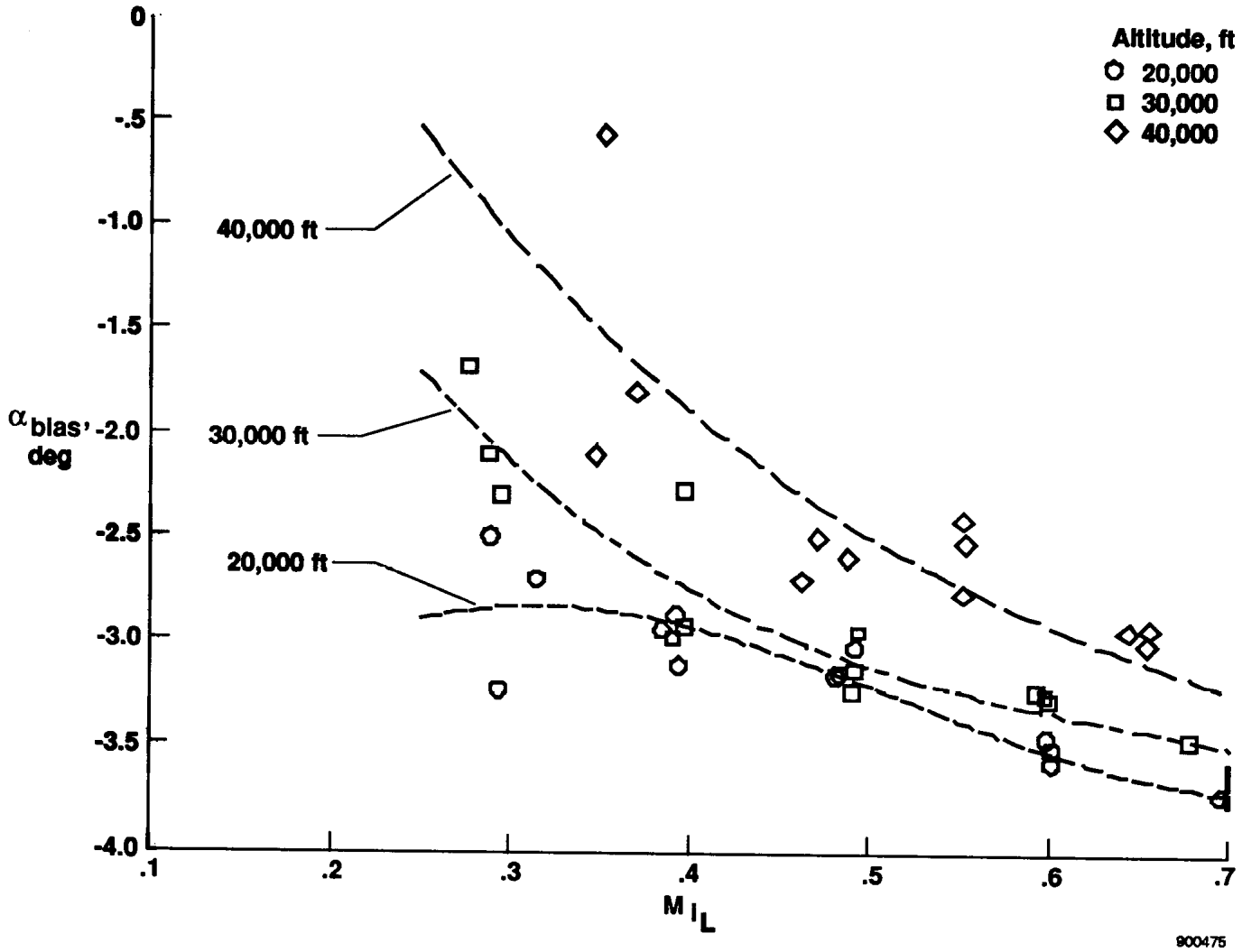

(b) α_{bias}.

Figure 14. Concluded.

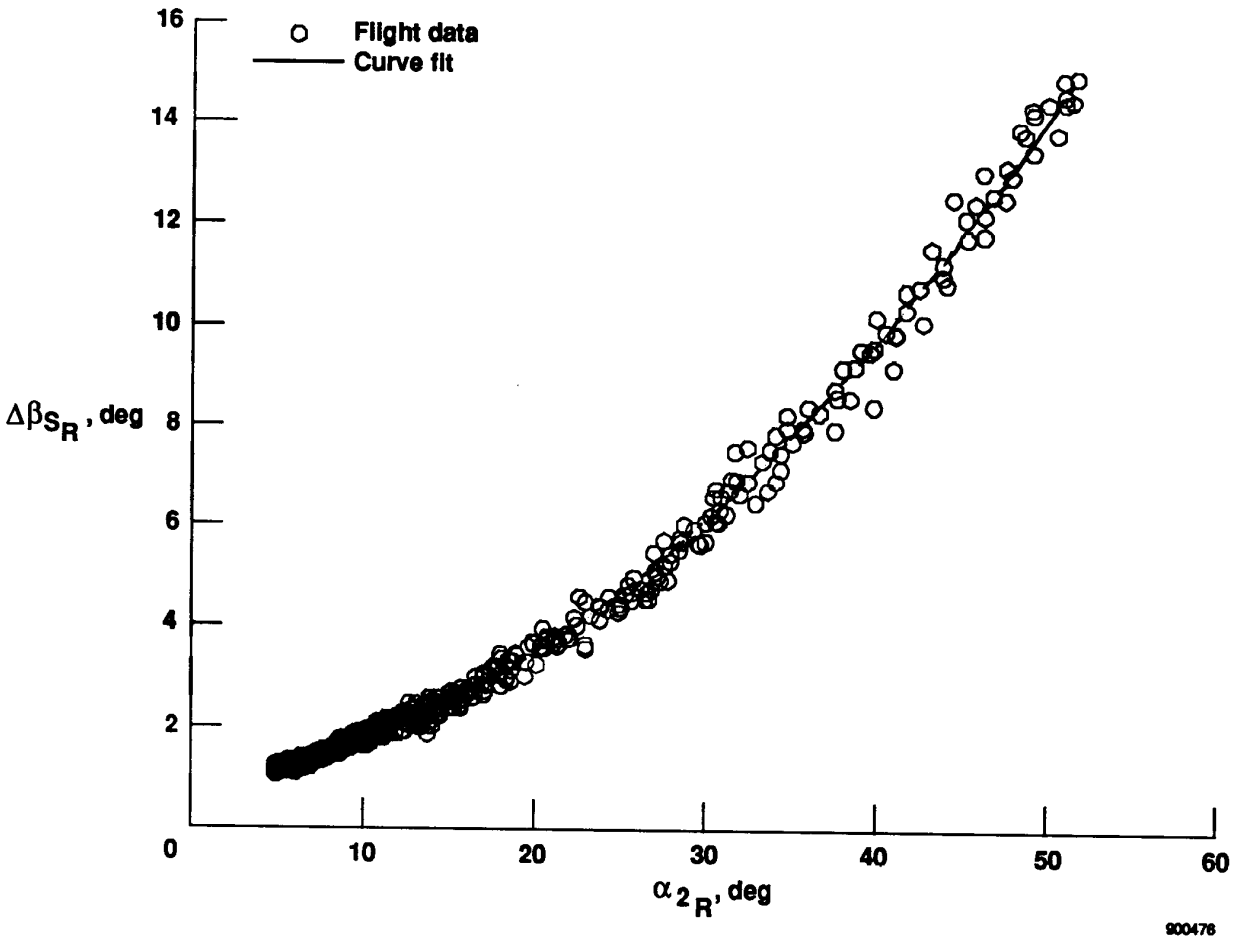

(a) Right wingtip probe.

Figure 15. Symmetric sidewash corrections for the angle-of-sideslip sensors.

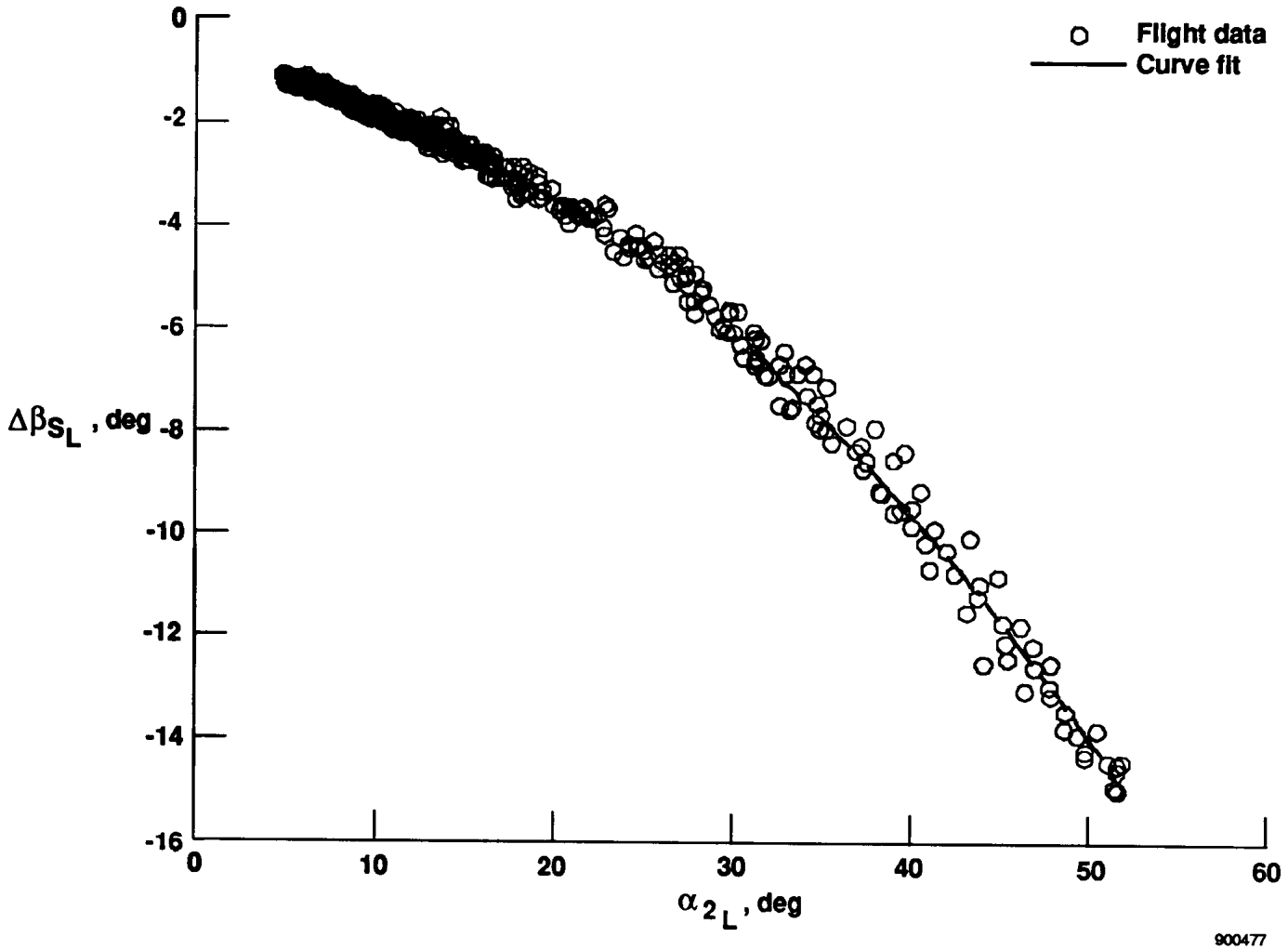

(b) Left wingtip probe.

Figure 15. Concluded.

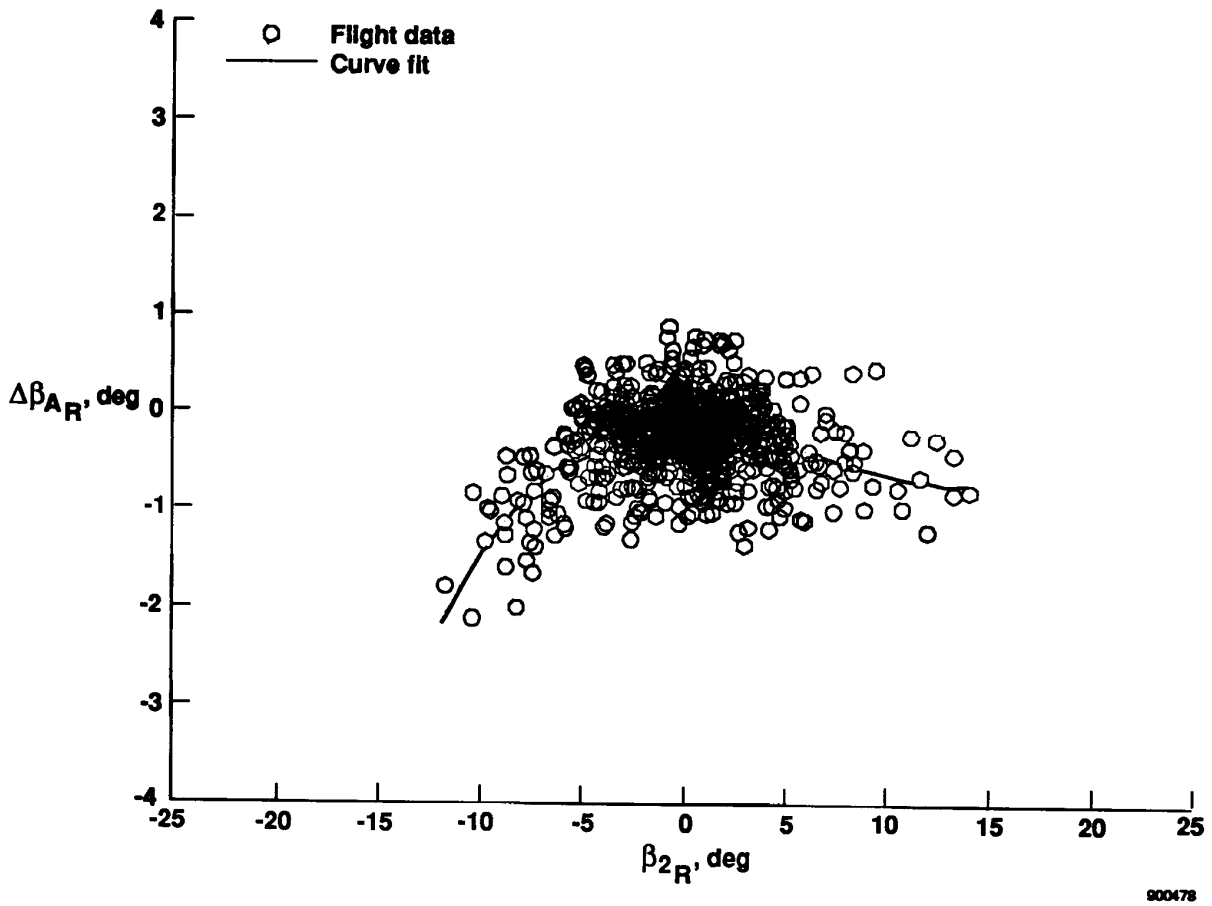

(a) Right wingtip probe.

Figure 16. Asymmetric sidewash corrections for the angle-of-sideslip sensors.

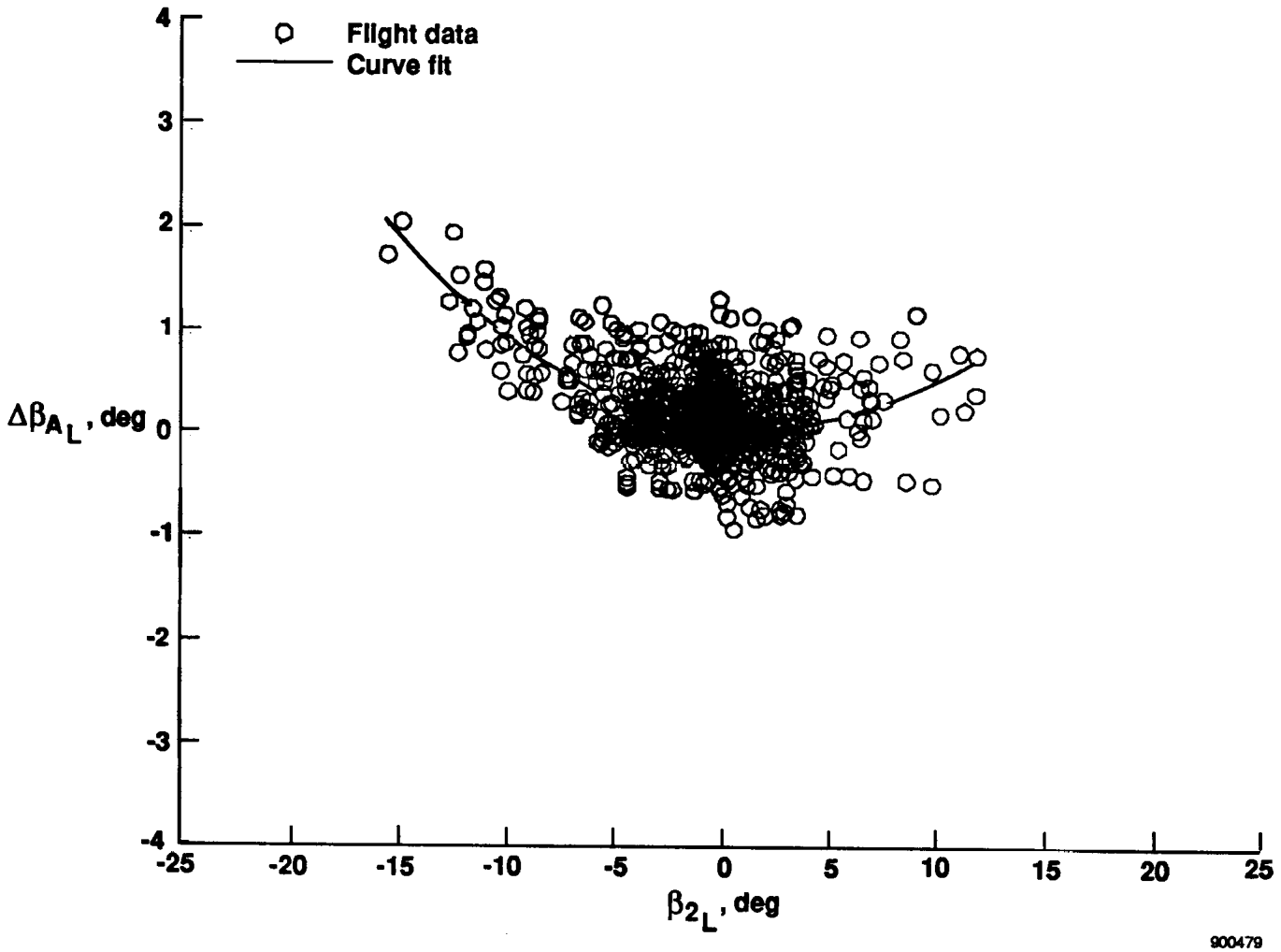

(b) Left wingtip probe.

Figure 16. Concluded.

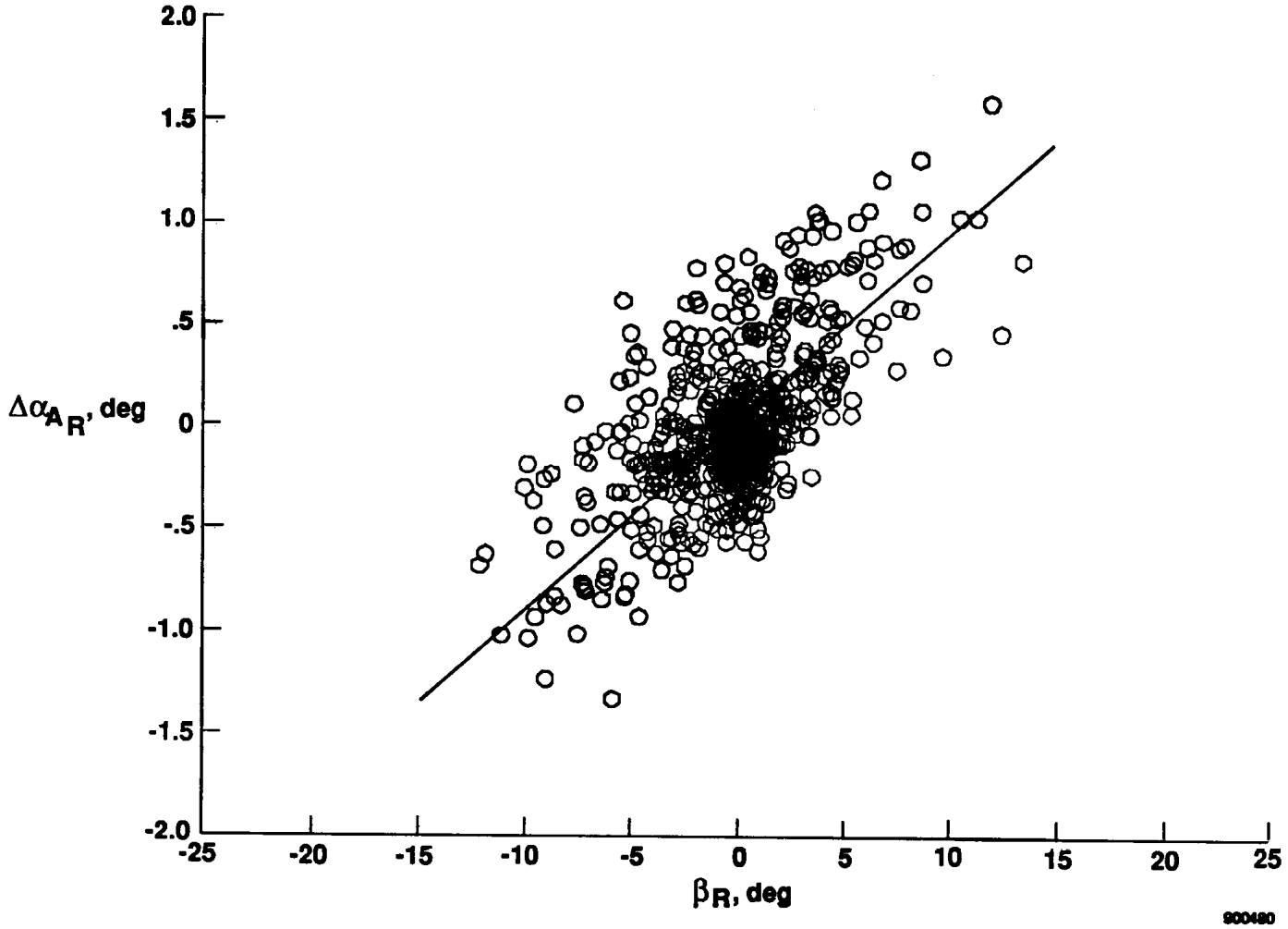

(a) Right wingtip probe.

Figure 17. Asymmetric upwash corrections for the angle-of-attack sensors.

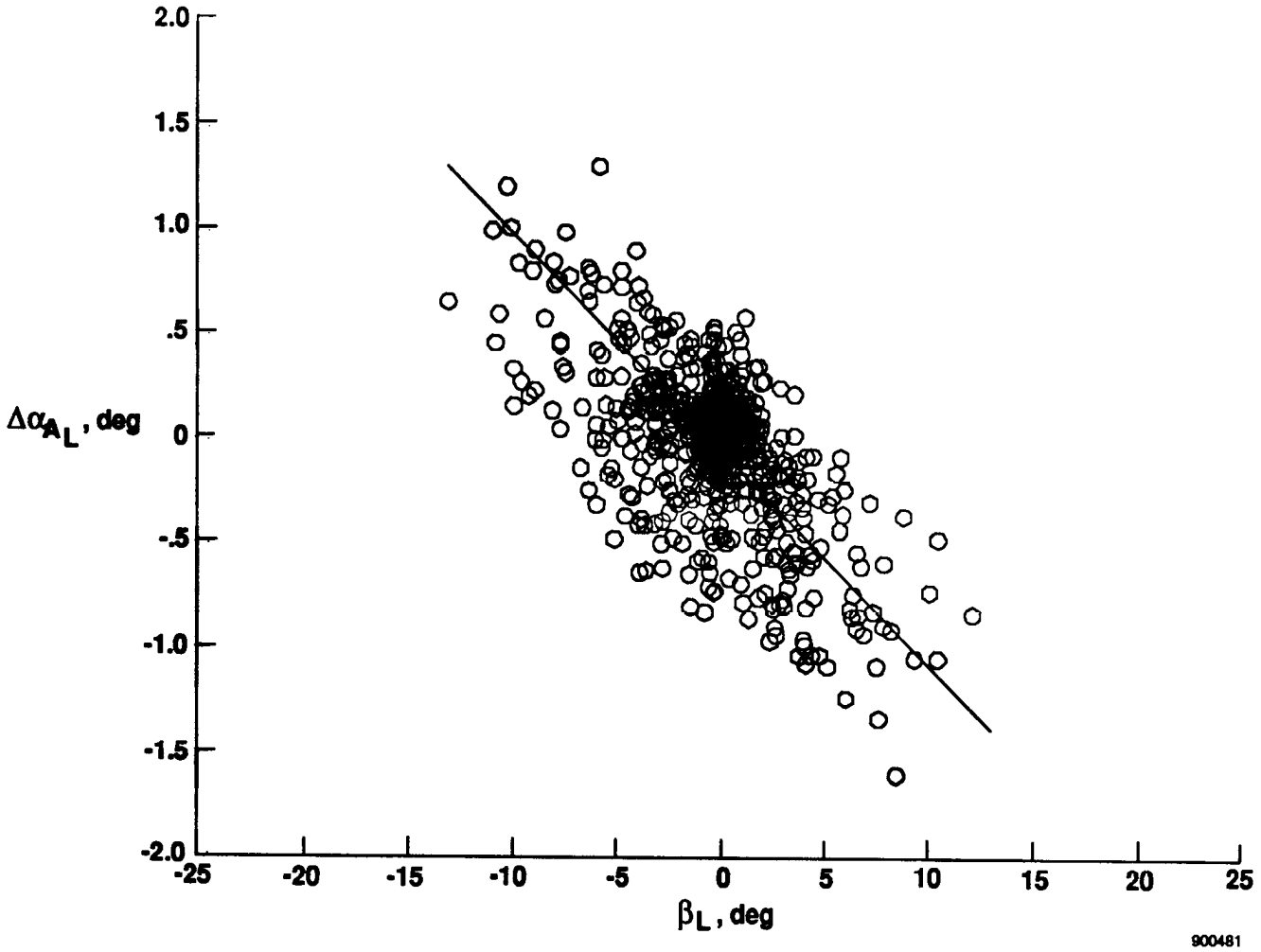

(b) Left wingtip probe.

Figure 17. Concluded.

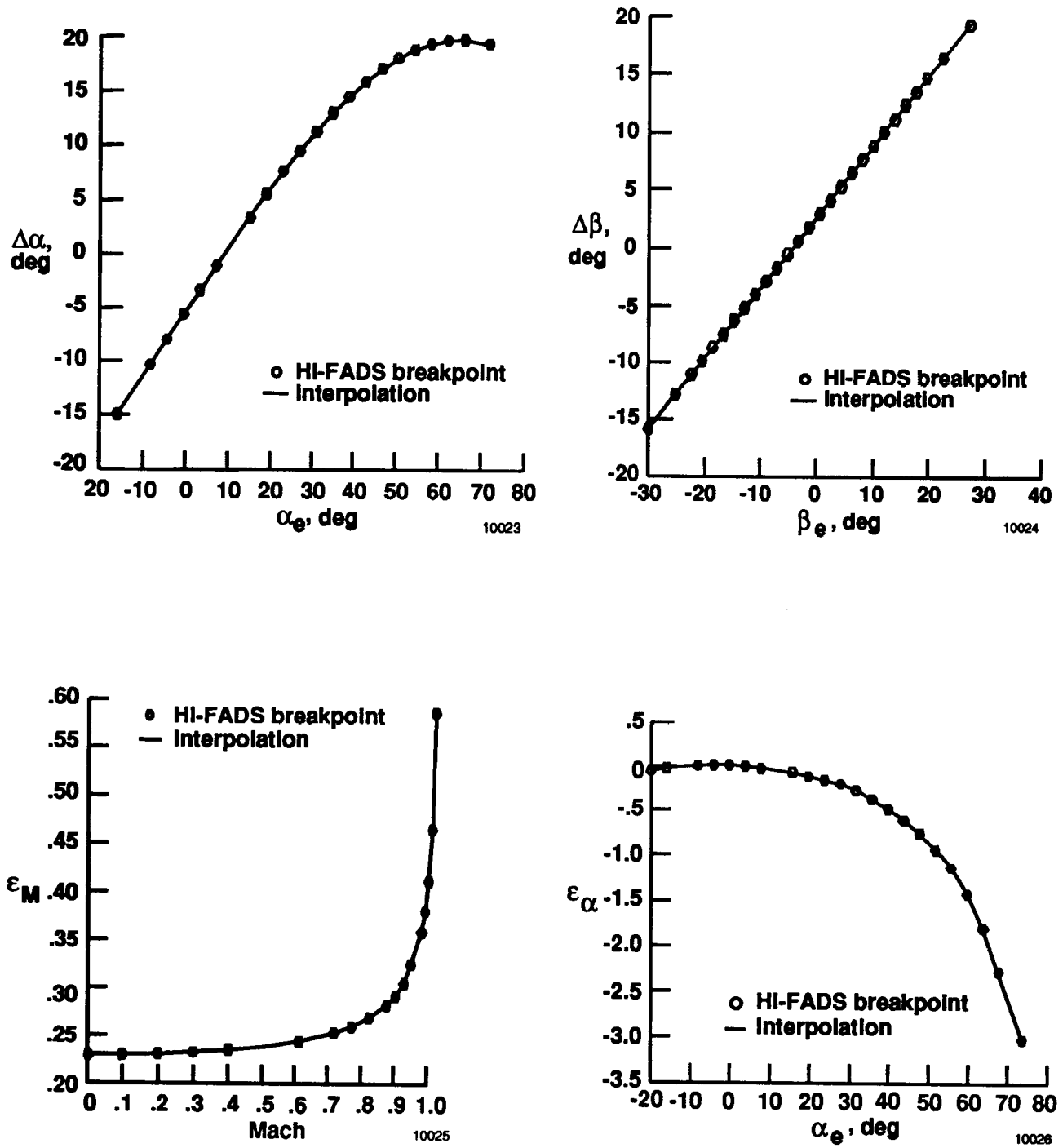

Figure 18. HI-FADS calibration parameters.

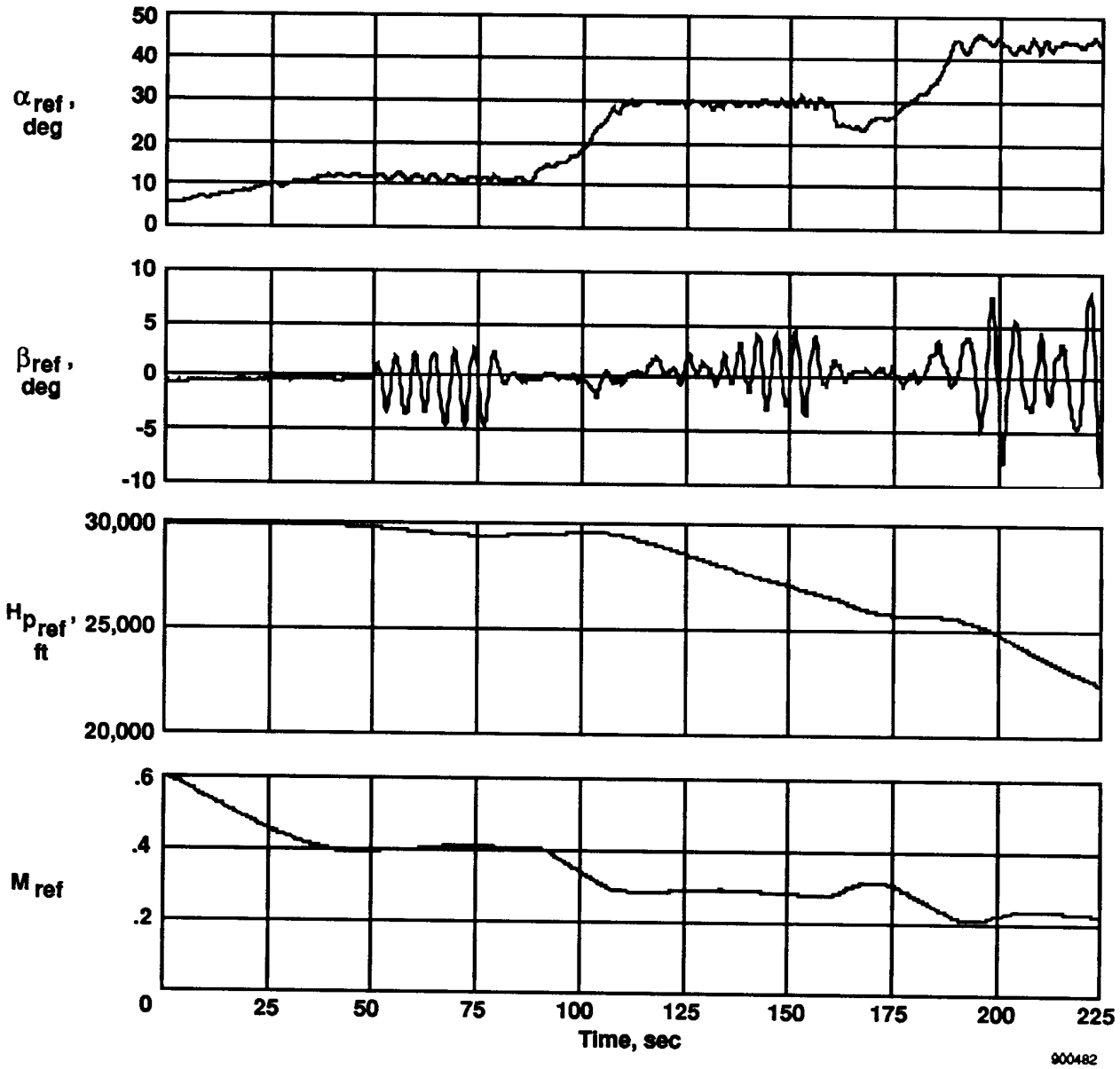

Figure 19. Time history of typical high angle-of-attack flight maneuver.

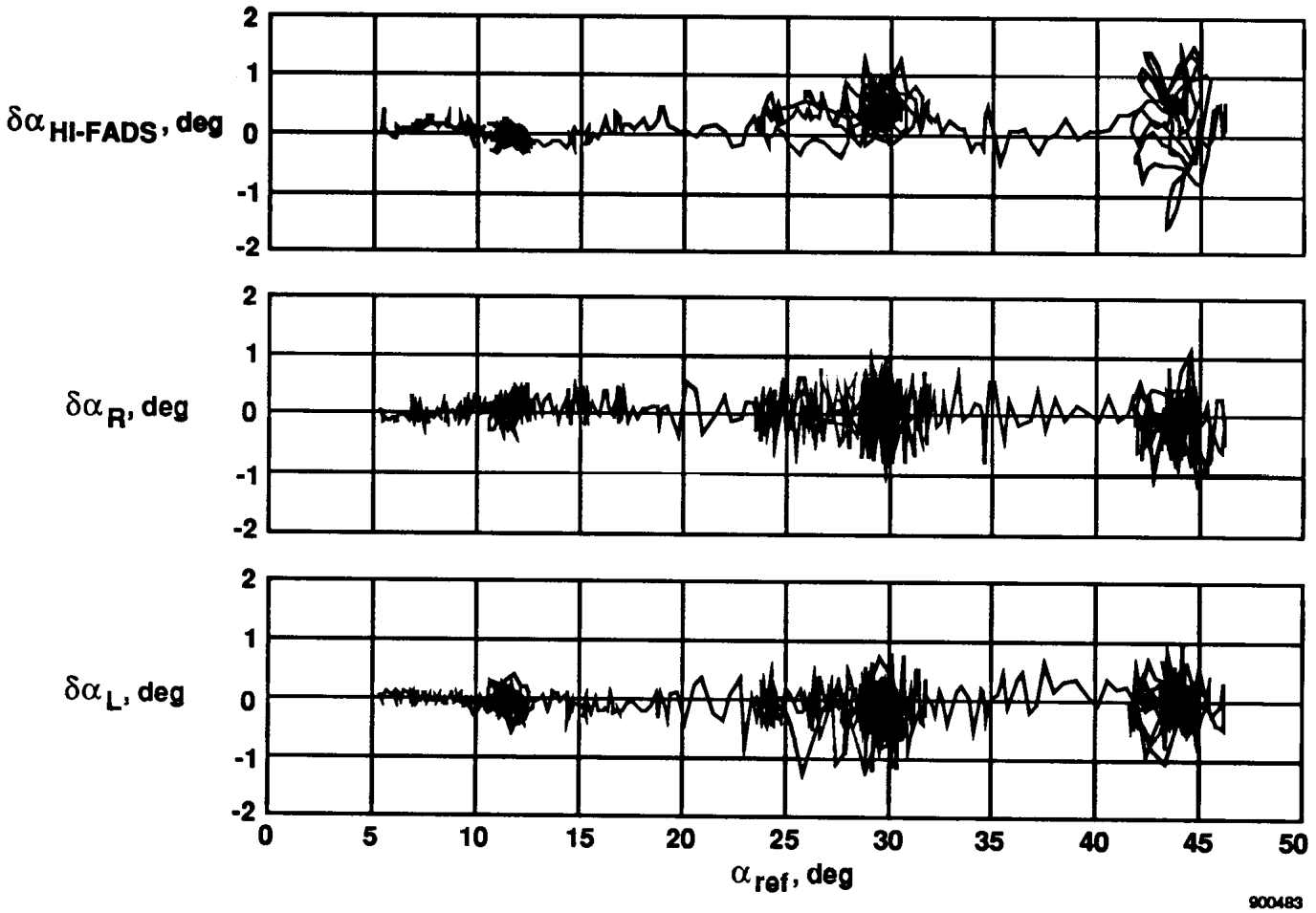

(a) Angle-of-attack residuals.

Figure 20. Residuals between the airdata system measurement and the reference measurement for the three airdata systems.

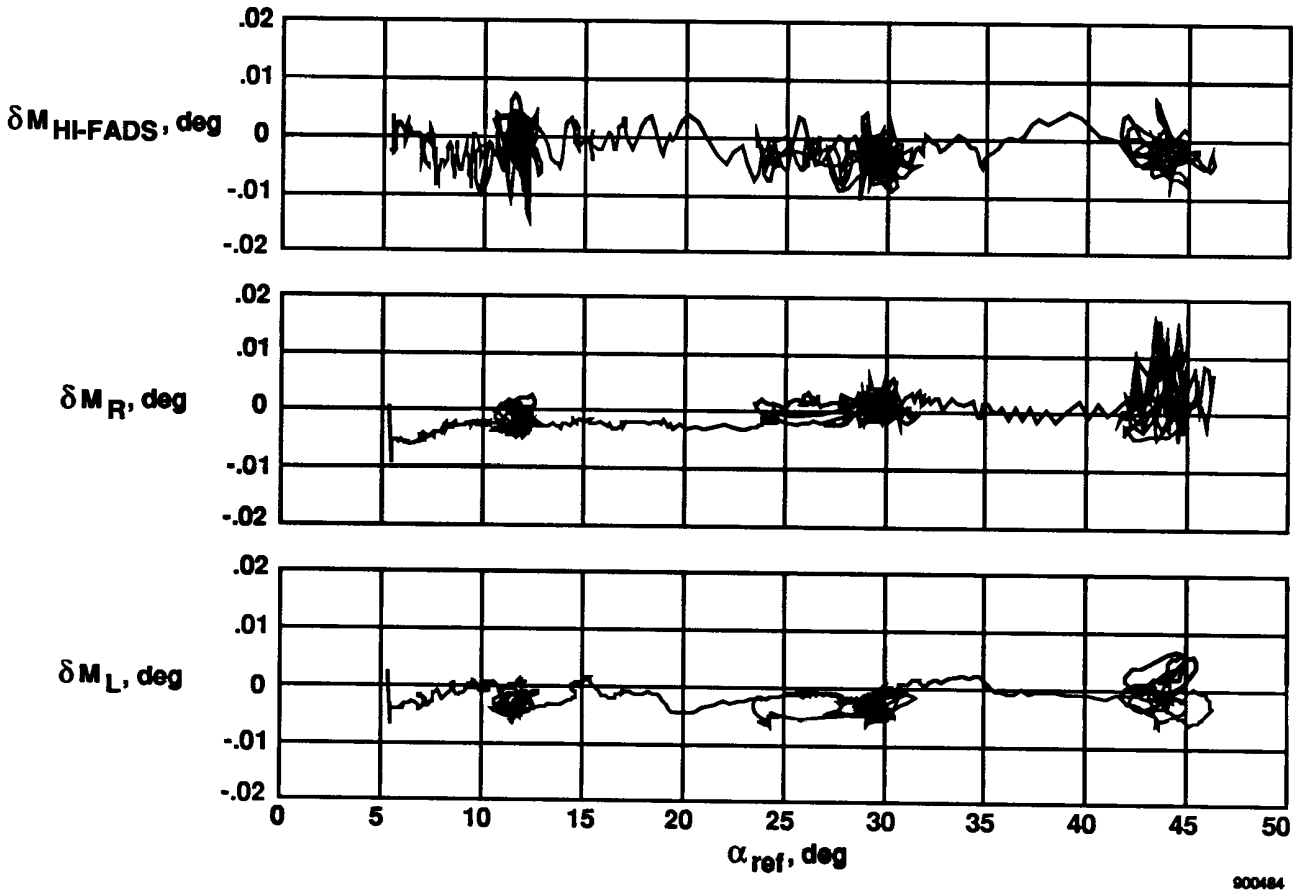

(b) Mach residuals.

Figure 20. Concluded.

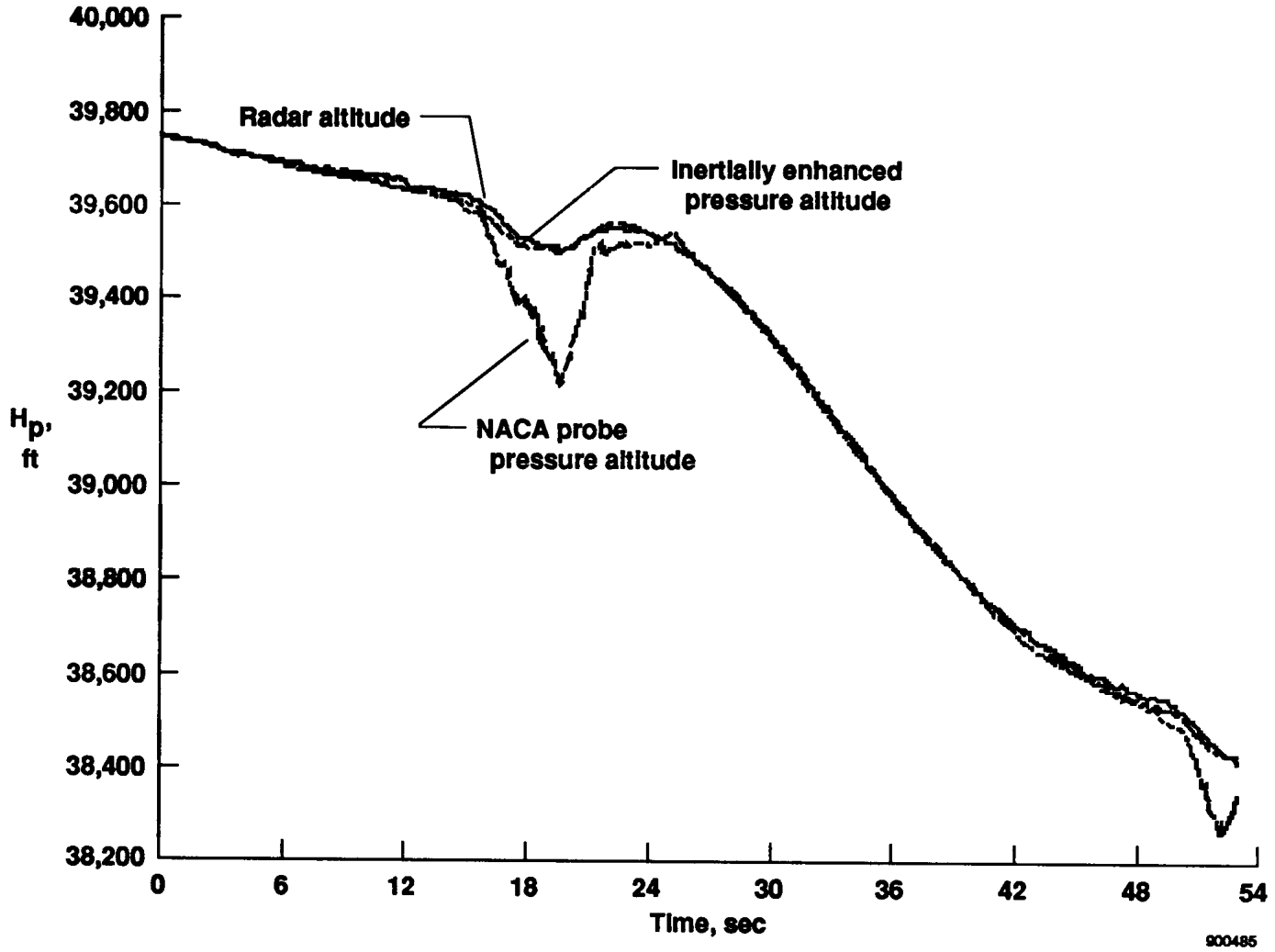

Figure 21. Time history of inertially enhanced NACA probe pressure altitude.

NASA
National Aeronautics and Space Administration

Report Documentation Page

1. Report No. NASA TM-101729	2. Government Accession No.	3. Recipient's Catalog No.
4. Title and Subtitle A Preliminary Look at Techniques Used to Obtain Airdata From Flight at High Angles of Attack		5. Report Date December 1990
		6. Performing Organization Code
7. Author(s) Timothy R. Moes and Stephen A. Whitmore		8. Performing Organization Report No. H-1674
		10. Work Unit No. RTOP 533-02-01
9. Performing Organization Name and Address NASA Ames Research Center Dryden Flight Research Facility P.O. Box 273, Edwards, California 93523-0273		11. Contract or Grant No.
12. Sponsoring Agency Name and Address National Aeronautics and Space Administration Washington, DC 20546-3191		13. Type of Report and Period Covered Technical Memorandum
		14. Sponsoring Agency Code

15. Supplementary Notes

Presented at the High Angle of Attack Technology Symposium, Hampton, Virginia, October 30 - November 1, 1990.

16. Abstract

Flight research at high angles of attack has posed new problems for airdata measurements. New sensors and techniques for measuring the standard airdata quantities of static pressure, dynamic pressure, angle of attack, and angle of sideslip were subsequently developed. This report updates the ongoing airdata research supporting NASA's F-18 high alpha research program. Included are the techniques used and the preliminary results. The F-18 aircraft was flown with three research airdata systems: a standard airdata probe on the right wingtip, a self-aligning airdata probe on the left wingtip, and flush airdata system on the nose cone. The primary research goal was to obtain steady-state calibrations for each airdata system up to an angle of attack of 50°. This goal was accomplished and preliminary accuracies of the three airdata systems were assessed and are presented in this report. An effort to improve the fidelity of the airdata measurements during dynamic maneuvering is also discussed. This involved enhancement of the aerodynamic data with data obtained from linear accelerometers, rate gyros, and attitude gyros. Preliminary results of this technique are presented.

17. Key Words (Suggested by Author(s)) Airdata FADS High angle of attack		18. Distribution Statement Unclassified-Unlimited Subject category 06	
19. Security Classif. (of this report) Unclassified	20. Security Classif. (of this page) Unclassified	21. No. of Pages 51	22. Price A04

NASA FORM 1626 OCT 86

For sale by the National Technical Information Service, Springfield, Virginia 22161-2171